

Dictionary-free Koopman model predictive control with nonlinear input transformation

Vít Cibulka^{1,2}, Milan Korda^{1,2}, and Tomáš Haniš¹

¹Department of Control Engineering, Faculty of Electrical Engineering, Czech Technical University in Prague, The Czech Republic

vit.cibulka@fel.cvut.cz, tomas.hanis@fel.cvut.cz

²CNRS, Laboratory for Analysis and Architecture of Systems, Toulouse, France
korda@laas.fr

September 22, 2023

Abstract

This paper introduces a method for data-driven control based on the Koopman operator model predictive control. Unlike existing approaches, the method does not require a dictionary and incorporates a nonlinear input transformation, thereby allowing for more accurate predictions with less ad hoc tuning. In addition to this, the method allows for input quantization and exploits symmetries, thereby reducing computational cost, both offline and online. Importantly, the method retains convexity of the optimization problem solved within the model predictive control online. Numerical examples demonstrate superior performance compared to existing methods as well as the capacity to learn discontinuous lifting functions.

1 Introduction

The Koopman operator approach is a successful framework for data-driven analysis of nonlinear dynamical systems that originated in the 1930s in the seminal works [18, 19] but gained wider popularity only much later in the mid 2000s with the advent of modern-day computing, starting with the works [25, 26]. The core idea is to represent the nonlinear system by an infinite-dimensional linear operator acting on the space of functions defined on the state-space (referred to as observables). Finite-dimensional approximations of this operator, computable from data using simple linear algebraic tools, then allow one to gain insight into the underlying dynamics and construct reduced-order models. This approach can be thought of as lifting of the original nonlinear dynamics into a higher dimensional space where it admits a linear description.

Generalizing this concept to control systems is far from trivial. A promising approach proposed in [21] defined the Koopman operator with control as acting on the product of the state-space

*This work has been supported by the Czech Science Foundation (GACR) under contract No. 20-11626Y, and by the Grant Agency of the Czech Technical University in Prague, grant No. SGS22/166/OHK3/3T/13. This work has also been supported by the AI Interdisciplinary Institute ANITI funding, through the French “Investing for the Future PIA3” program under the Grant agreement n° ANR-19-PI3A-0004 as well as by the National Research Foundation, Prime Minister’s Office, Singapore, under its Campus for Research Excellence and Technological Enterprise (CREATE) programme.

** This work has been submitted to SIAM Journal on Applied Dynamical Systems (SIADS) and is currently under review.

and the space of all control sequences and used finite-dimensional approximations of this operator within a linear model predictive control scheme, nowadays referred to as the Koopman MPC. The primary benefit is the convexity of the MPC problem solved online with computational complexity compared to classical linear MPC. The primary drawback is the inherent limitation of prediction accuracy. Indeed, the predictors proposed in [21] lift only the state whereas the control input remains untransformed and enters linearly into the predictor used within the MPC in order to preserve convexity. Therefore, fixing an initial condition, the mapping from the control input sequence to the output of the predictor is linear whereas the true mapping realized by the nonlinear system is typically nonlinear. A possible remedy is to consider bilinear predictors, which has a long history related to generalizing the classical Carleman linearization [9] to a controlled setting; see, e.g., [13, 30, 3, 33]. This, however, necessarily spoils the convexity of the MPC problem solved online and is hence not pursued in this work. We refer the reader to the survey [8] for further discussion regarding the use of the Koopman operator in control.

A second drawback, common in controlled and uncontrolled settings, is the need for a user-specified dictionary of nonlinear lifting functions. Although such dictionaries may be naturally available for measure-preserving ergodic systems in the form of time-delayed measurements of the state [2], no such choice is available in more general settings and hence past works resorted to ad-hoc dictionaries (e.g., [36, 21]) such as radial basis functions or monomials. Even though efforts have been made to alleviate this by using a general parametrization of the dictionary (e.g., with neural networks [23]) or by exploiting the dynamics and state-space geometry to construct them [20], the need for a significant engineering effort in the design process has not been eliminated.

This work addresses the two principal issues described above as well as demonstrates how input quantization and symmetries of the problem can be exploited. Specifically, we first propose a class of predictors with nonlinear input transformation that preserves convexity of the MPC problem solved online and greatly improves the long-term prediction accuracy. To the best of our knowledge this is the first time that a nonlinear input transformation is employed while preserving convexity of the MPC problem.

Second, we eliminate the need for a dictionary by treating the values of the lifting functions on the available data samples as optimization variables in the (offline) learning process. Concurrently with our work, a different dictionary-free method for construction of Koopman predictors was developed in [27] using hidden Markov models; however, albeit providing accurate predictions, the models constructed therein are bilinear and hence lead to nonconvex problems when used within MPC.

In addition to this, we allow for input quantization, thereby bringing the method closer to practical applications where the control input is typically quantized.

Finally, we exploit symmetries in designing the predictors, thereby allowing for a more parsimonious parametrization of the predictors and hence faster learning; this could be seen as a generalization of the symmetry-exploitation methods without control proposed in [31] to the controlled setting where the interplay between state-space and control-space symmetries must be carefully taken into account.

We demonstrate the effectiveness of our approach on several examples, including the highly nonlinear vehicle model adopted from our previous work in [10]. The current research around the Koopman operator for vehicle control includes [34] and [35], which both use the method [21] and therefore require user-specified dictionary for the state lifting. On the other hand, the work [10] does not require an explicit dictionary of lifting functions but it still involves a notable engineering effort to construct the state lifting. Our paper uses the same vehicle model as [10], while minimizing the effort to construct the state lifting and, for the first time, employs input lifting. The proposed Koopman MPC significantly outperforms the previous methods on this vehicle model and, interestingly, the analysis of the input lifting functions unveils certain physical properties that can be directly tied to the vehicle dynamics.

Structure of this paper The Section 2 provides the problem statement and the Section 3 presents the main result of this paper. Then we discuss symmetry exploitations in the Section 4. Various implementation details of the method are presented in Section 5. The usage of the Koopman

operator in control is presented in the Section 6, and the concrete form of the Koopman MPC used in this paper is summarized in the Section 7. The numerical examples are presented in the Section 8 and we conclude in the Section 9.

Notation All vectors are assumed to be column vectors. The set of integers from 1 to n will be denoted as $\mathbb{Z}_{1,n}$. The cardinality of a set A is denoted as $|A|$. The identity matrix of size n is I_n ; the column vector of ones of size n is denoted as $\mathbf{1}_n$. The element-wise multiplication is denoted by \odot . A block-diagonal matrix with blocks x_1, \dots, x_n on the diagonal is denoted as $\text{bdiag}(x_1, \dots, x_n)$. For a vector x and a positive semidefinite matrix Q , we denote $\|x\|_Q := \sqrt{x^\top Q x}$.

2 Problem statement

Let us consider a discrete-time controlled nonlinear dynamical system

$$\begin{aligned} x_{t+1} &= f(x_t, u_t) \\ y_t &= g(x_t), \end{aligned} \quad (1)$$

where $x_t \in X \subset \mathbb{R}^{n_x}$, $u_t \in U \subset \mathbb{R}^{n_u}$, $y_t \in Y \subset \mathbb{R}^{n_y}$ are the state, the input, and the output vectors.

We define the Koopman operator \mathcal{K} with control input similarly as in [21], by considering the extended state-space $\mathbb{R}^{n_x} \times \ell(U)$, where $\ell(U) := \{(u_i)_{i=0}^\infty \mid u_i \in U\}$ is the space of all control sequences. We shall denote the elements of $\ell(U)$ by $\mathbf{u} := (u_i)_{i=0}^\infty$. The extended dynamics is defined by

$$\chi^+ = F(\chi) = \begin{bmatrix} f(x, \mathbf{u}(0)) \\ S\mathbf{u} \end{bmatrix}, \text{ for } \chi(0) = \begin{bmatrix} x_0 \\ \mathbf{u}_0 \end{bmatrix}, \quad (2)$$

where $\chi = (x, \mathbf{u}) \in \mathbb{R}^{n_x} \times \ell(U)$ is the extended state, $\mathbf{u}(0)$ denotes the first element of the sequence \mathbf{u} , and S is a shift operator such that $(S\mathbf{u})(i) = \mathbf{u}(i+1)$. The Koopman operator $\mathcal{K} : \mathcal{H} \rightarrow \mathcal{H}$ is then defined by

$$(\mathcal{K}\xi)(\chi) := \xi(F(\chi)) \quad (3)$$

for $\xi : \mathbb{R}^{n_x} \times \ell(U) \rightarrow \mathbb{R}$ that belongs to some space of observables \mathcal{H} . The functions ξ that the Koopman operator acts on are referred to as observables. In this work, we shall assume the observables in the form

$$\xi(\chi) = \begin{bmatrix} \Phi(x) \\ \Psi(\mathbf{u}(0)) \end{bmatrix}. \quad (4)$$

where $\Phi : X \rightarrow Z$ is a vector state lifting function, $\Psi : U \rightarrow V$ is the input transformation. The spaces $Z \subset \mathbb{R}^{n_z}$ and $V \subset \mathbb{R}^{n_v}$ are the Koopman state and input spaces respectively.

Note that with this definition, the operator \mathcal{K} will predict the future lifted inputs; we will disregard those since we are not interested in the spectral properties of the operator. Our goal is linear prediction of the controlled nonlinear dynamics (1).

Furthermore, since \mathcal{K} is generally infinite-dimensional, we will work with its finite-dimension truncation in the form of an LTI predictor

$$\begin{aligned} z_{t+1} &= Az_t + Bv_t \\ \hat{y}_t &= Cz_t, \quad \text{for } z_0 = \Phi(x_0) \text{ and } v_t = \Psi(u_t), \end{aligned} \quad (5)$$

where $A \in \mathbb{R}^{n_z \times n_z}$, $B \in \mathbb{R}^{n_z \times n_v}$, $C \in \mathbb{R}^{n_y \times n_z}$ are matrices to be determined. The system ((5)) is referred to as the *Koopman predictor*; the state z_t is referred to as the *lifted state* and \hat{y}_t is the predicted output of the system (1).

The primary goal of this work is to find A, B, C, Ψ, Φ , such that the resulting LTI system (5) predicts the behaviour of the nonlinear dynamics (1) on X for H_T steps ahead. This predictor is then used for controller synthesis within Koopman MPC, which we describe in Section 6.

3 Finding the Koopman predictor

In this section we present a method for determining the Koopman predictor ((5)). We start by giving an intuition: Assuming that we have trajectory data (y_t, u_t, x_0) for times $t \in \mathbb{Z}_{0, H_T}$, we want to find the linear system (5) so that its output \hat{y}_t matches the trajectory data y_t . The distinguishing feature of our work is that we do so in a *dictionary-free* manner, that is, by optimizing the values of Φ and Ψ on the available data without having to specify a dictionary of basis functions parametrizing Φ and Ψ . In addition to optimizing the values of Φ and Ψ , we also optimize over the system matrices A, B, C . See Figure 1 for an illustration.

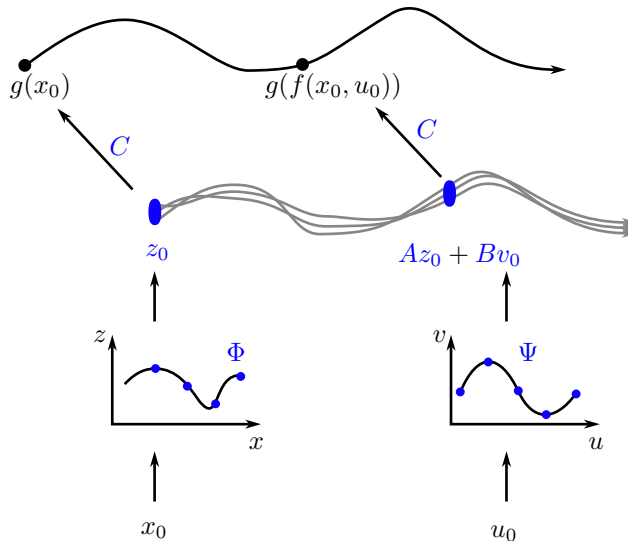


Figure 1: The intuition behind the Koopman predictor with control. Both the initial state and the inputs are lifted via the functions Φ and Ψ respectively. The linearly evolving high-dimensional trajectory of the Koopman predictor (5) can then be projected onto the original state space, giving us the nonlinear trajectory of (1). The quantities optimized in our approach are highlighted in blue; this includes the values of Φ and Ψ on the available data.

Basic definitions

The optimization will be done over N trajectories of the nonlinear system (1). To define the trajectories, we first need to define the sets of initial conditions and admissible system inputs.

We will assume to have samples x_0^i from X , which are the initial states of the aforementioned trajectories of (1)

$$X_0 = \{x_0^i \in X : i \in \mathbb{Z}_{1, N}\}. \quad (6)$$

To each $x_0^i \in X$, we associate a lifted initial condition $z_0^i \in Z_0 \subset \mathbb{R}^{n_z}$; these will be decision variables in the optimization problem where the control Koopman predictor is learned.

We will consider each input channel of the system (1) individually and assume that it is normalized to $[-1, 1]$. We also permit quantization of the control signal, thereby taking into account a digital control implementation or control signals that are discrete in nature (e.g., gears in a vehicle). The k^{th} input channel with q_k quantization levels reads

$$U_k \subset [-1, 1], \quad |U_k| = q_k. \quad (7)$$

The full input space can be retrieved as the cartesian product of the individual channels

$$U = U_1 \times U_2 \times \dots \times U_{n_u}. \quad (8)$$

In the optimization process, we will be searching for the transformed input channels V_k , which have the same number of quantization levels as U_k :

$$V_k \subset [V_{k,\min}, V_{k,\max}], \quad |V_k| = q_k. \quad (9)$$

We do not make assumptions on the maxima and minima of the lifted input channels, since they are optimization variables.

After finding the Koopman predictor, we can retrieve the lifted input space as

$$V = V_1 \times V_2 \times \dots \times V_{n_u}. \quad (10)$$

We will assume that the dimensions of both the original and lifted inputs are the same, i.e. $n_v = n_u$. Although this assumption is not required by the algorithm itself, the benefit of raising the input dimension is not investigated in this paper. The values V_k are decision variables to optimize.

The Example 1 shows the advantage of considering the inputs channel-by-channel, instead of working with the whole cartesian product (8).

Example 1. Assume that we have two input channels quantized as

$$U_1 = \{-1, 1\}, U_2 = \{-1, 0.4, 1\}, \quad (11)$$

with $q_1 = 2$ and $q_2 = 3$. We retrieve U as

$$U = \left\{ \begin{bmatrix} -1 \\ -1 \end{bmatrix}, \begin{bmatrix} 1 \\ -1 \end{bmatrix}, \begin{bmatrix} -1 \\ 0.4 \end{bmatrix}, \begin{bmatrix} 1 \\ 0.4 \end{bmatrix}, \begin{bmatrix} -1 \\ 1 \end{bmatrix}, \begin{bmatrix} 1 \\ 1 \end{bmatrix} \right\}. \quad (12)$$

Optimizing over the channels V_1 and V_2 will introduce $\sum_k q_k = 5$ optimization variables. Should we, however, optimize over the whole set V , we would have $n_u \prod_k q_k = 12$ variables. Considering each channel individually decreases the parameter space of the optimization and therefore increases the scalability of the algorithm. It also makes it easier to enforce invertibility of the transformation Ψ , which is crucial in control applications. This is discussed further in Section 6.2.4.

Representation of quantized inputs All the input vectors considered further in this section are elements of either U or V , and can be represented by a linear operator $\mathcal{L} : \mathbb{R}^{\sum_k q_k} \rightarrow \mathbb{R}^{n_u}$. Let us assume that we have an input $u' \in U$ and a corresponding lifted input $v' \in V$. We can write u' as

$$u' = \mathcal{L}'(U_1, U_2, \dots, U_{n_u}), \quad (13)$$

where \mathcal{L}' selects appropriate values from the channels U_k in order to build the vector u' . The same operator can be used for the lifted vector v' as

$$v' = \mathcal{L}'(V_1, V_2, \dots, V_{n_u}). \quad (14)$$

Action of a linear operator can be represented by matrix multiplication; we shall represent the operator \mathcal{L} by a matrix L . For u' we get

$$u' = L' [U_1^\top \quad U_2^\top \quad \dots \quad U_{n_u}^\top]^\top \quad (15)$$

and similarly for v' , with the same matrix L' . The matrix L (and L') is a block-diagonal matrix with row one-hot vectors on the diagonal, selecting only one element from each channel; it shall be referred to as *projection matrix*.

The Example 2 demonstrates the linear mapping via the projection matrix L .

Example 2. Assume $u' = [-1 \ 0.4]^\top$, $U_1 = \{-1, 1\}$, and $U_2 = \{-1, 0.4, 1\}$. The equation (15) would then look as

$$u' = L' \begin{bmatrix} U_1 \\ U_2 \end{bmatrix} \quad (16)$$

$$\begin{bmatrix} -1 \\ 0.4 \end{bmatrix} = \begin{bmatrix} [1 & 0] & 0 & 0 & 0 \\ 0 & 0 & [0 & 1 & 0] \end{bmatrix} \begin{bmatrix} -1 \\ 1 \\ -1 \\ 0.4 \\ 1 \end{bmatrix},$$

therefore $L' = \text{bdiag}([1 \ 0], [0 \ 1 \ 0])$.

Assume that we have the lifted input channels defined as $V_1 = \{1, 0.2\}$, and $V_2 = \{4, 3, 0.1\}$. We can calculate the lifted vector v' which corresponds to u' by using the same matrix L' as

$$v' = L' \begin{bmatrix} V_1 \\ V_2 \end{bmatrix} = \begin{bmatrix} [1 & 0] & 0 & 0 & 0 \\ 0 & 0 & [0 & 1 & 0] \end{bmatrix} \begin{bmatrix} 1 \\ 0.2 \\ 4 \\ 3 \\ 0.1 \end{bmatrix} = \begin{bmatrix} 1 \\ 3 \end{bmatrix}. \quad (17)$$

The correspondence between u' and v' is therefore explicitly established by sharing the same projection matrix L' .

Dataset for learning A dataset of N trajectories of the system (1) is denoted as \mathcal{D} where a single trajectory $\mathcal{T}_i \in \mathcal{D}$ with initial condition $x_0^i \in X_0$ and length H_T is defined as

$$\begin{aligned} \mathcal{T}_i &= \{(x_s^i, u_s^i, y_s^i) \in X \times U \times Y \\ &\text{s.t. } x_{s+1}^i = f(x_s^i, u_s^i) \quad \forall s \in 0 \dots H_T - 1 \\ &\quad y_s^i = g(x_s^i) \quad \forall s \in 0 \dots H_T \\ &\text{and } u_s^i = L_s^i [U_1^\top \ \dots \ U_{n_u}^\top]^\top\}, \end{aligned} \quad (18)$$

where L_s^i is a projection matrix associated with the input u_s^i .

Lifting functions We will obtain the state lifting function $\Phi : \mathbb{R}^{n_z} \rightarrow \mathbb{R}^{n_x}$ by pairing the vectors x_0^i and z_0^i as

$$z_0^i = \Phi(x_0^i) \quad \forall i \in \mathbb{Z}_{1,N}, \quad (19)$$

where $z_0^i \in Z_0$ and $x_0^i \in X_0$. In this way, we obtain the function Φ on N samples. This function is subsequently extended to all of X through interpolation; this is detailed in Section 6.2.3.

Due to the channel separation, the input lifting function Ψ is built by concatenating individual functions $\Psi_k : \mathbb{R} \rightarrow \mathbb{R}$. The j^{th} element of the k^{th} channel input vector is transformed as

$$\begin{aligned} v_k^j &= \Psi_k(u_k^j) \quad \forall j \in \mathbb{Z}_{1,q_k}, \\ &\text{where } u_k^j \in U_k, v_k^j \in V_k. \end{aligned} \quad (20)$$

We can write $\Psi : \mathbb{R}^{n_u} \rightarrow \mathbb{R}^{n_u}$ as

$$\begin{bmatrix} v_1 \\ \vdots \\ v_{n_u} \end{bmatrix} = \begin{bmatrix} \Psi_1(u_1) \\ \vdots \\ \Psi_{n_u}(u_{n_u}) \end{bmatrix}. \quad (21)$$

With the definitions (19) and (21), optimizing over samples of Z_0 and V_k could be viewed as optimizing over the image of the lifting functions Φ and Ψ respectively.

3.1 Optimization problem setup

As a reminder, the output of the linear system (5) at time k for initial condition $z_0^i \in Z_0$ is

$$\hat{y}_t^i = C \left(A^t z_0^i + \sum_{j=0}^{t-1} A^{t-1-j} B v_j \right) \quad (22)$$

To find the Koopman predictor, we will seek to solve the problem

$$\begin{aligned} & \text{minimize} \sum_{i=0}^N \sum_{t=0}^{H_T} \|C z_t^i - y_t^i\|_2^2 + w_0 \sum_{(a,b) \in \mathcal{S}} \|z_{H_T}^a - z_0^b\|_2^2 + \theta(\cdot) \\ & \text{s.t. } z_t^i = \left(A^t z_0^i + \sum_{j=0}^{t-1} A^{t-1-j} B v_j^i \right) \\ & v_j^i = L_j^i [V_1^\top \quad \dots \quad V_{n_u}^\top]^\top \end{aligned} \quad (23)$$

where A, B, C, z_0^i, V_k are the decision variables, $\mathcal{S}, L_j^i, y_t^i \in \mathcal{D}$ are the problem data, and H_T and N are the trajectory length and number of trajectories respectively. The scalar w_0 is a weighting parameter. The set \mathcal{S} contains indices of consecutive trajectories so for any $(a, b) \in \mathcal{S}$, \mathcal{T}_a ends at the same point where \mathcal{T}_b begins; the reasoning behind this regularization is explained further below, in the Section 5.1.

The first term in the cost function ensures the fit of the data; the second one promotes invariance of Z_0 by connecting the consecutive trajectories in the lifted space, it can also be thought of as a regularization term. The last term, θ , is a placeholder for optional regularization, such as enforcing invertibility and symmetry of the input transformation Ψ which is discussed in the Section 5 and below Corrolary 1 respectively. The problem (23) can be simplified in terms of the number of variables and data requirements by exploiting symmetries of system (1), which will be discussed in the next section.

4 Exploiting symmetry

Assuming that the nonlinear system (1) has a symmetry, we can exploit this symmetry in our algorithm to decrease the size of the dataset by imposing structure onto the matrices (A, B, C) , which will guarantee that the Koopman predictor will respect the same symmetries as (1). This means that the learning dataset \mathcal{D} will not need to contain symmetric trajectories, since the symmetry will be implicitly enforced by the structure of (A, B, C) , thus decreasing the size of \mathcal{D} , Z_0 , and the number of decision variables in (A, B, C) .

We consider state-control symmetries with respect to groups $\Gamma^x \subset \text{GL}_{n_x}$ and $\Gamma^u \subset \text{GL}_{n_u}$, where GL_n denotes the group of invertible matrices of size n -by- n . The group elements are denoted by $\gamma^x \in \Gamma^x$ and $\gamma^u \in \Gamma^u$ and the group action is the standard matrix multiplication. The two groups

are assumed to be related by a group homomorphism $h : \Gamma^x \rightarrow \Gamma^u$, i.e., $h(\gamma_1^x \gamma_2^x) = h(\gamma_1^x)h(\gamma_2^x)$. A dynamical system is said to have a symmetry with respect to (Γ^x, Γ^u, h) if for all $\gamma^x \in \Gamma^x$ it holds

$$f(\gamma^x x, \gamma^u u) = \gamma^x f(x, u), \quad (24)$$

where $\gamma^u = h(\gamma^x)$. Our goal is to find a linear predictor whose output will respect the symmetry with respect to Γ^x . In order to do so, we will construct a symmetry group $\Gamma^z \subset \text{GL}_{n_z}$ and a group homomorphism $h' : \Gamma^x \rightarrow \Gamma^z$ such that

$$\begin{aligned} A\gamma^z z + B\gamma^u v &= \gamma^z (Az + Bv) \\ C\gamma^z z &= \gamma^x Cz \end{aligned} \quad (25)$$

for all $\gamma^x \in \Gamma^x$, where $\gamma^z = h'(\gamma^x)$ and $\gamma^u = h(\gamma^x)$. This implicitly assumes that the input symmetries are the same for the original system and the predictor; the requirements on the transformations Φ and Ψ for this to hold are stipulated later in Corollary 1.

To simplify the exposure, this section assumes that the output of the predictor (25) is prediction of the nonlinear state x . Furthermore, we shall consider only sign symmetries, meaning that $(\Gamma^x, \Gamma^u, \Gamma^z)$ are subsets of diagonal matrices with $+1$ or -1 on the diagonal.

We shall simplify the notation by denoting the diagonal matrices as vectors containing the diagonal whenever clear from the context.

Example 3. Assume the following discrete dynamical system $x^+ = f(x, u)$ (we drop the index k for readability):

$$\begin{aligned} x_1^+ &= -x_1 u_1 - |x_2| \\ x_2^+ &= -x_2 + u_2 + u_3 \\ x_3^+ &= -x_3 |x_2| + u_2 + u_3 \\ x_4^+ &= -x_4. \end{aligned} \quad (26)$$

The set Γ^x is

$$\Gamma^x = \left\{ \begin{bmatrix} 1 \\ 1 \\ 1 \\ 1 \end{bmatrix}, \begin{bmatrix} 1 \\ -1 \\ -1 \\ 1 \end{bmatrix}, \begin{bmatrix} 1 \\ 1 \\ 1 \\ -1 \end{bmatrix}, \begin{bmatrix} 1 \\ -1 \\ -1 \\ -1 \end{bmatrix} \right\} \quad (27)$$

and the pairs (γ^x, γ^u) can take following values:

$$\begin{aligned} (\gamma^x, \gamma^u) &= (\gamma^x, h(\gamma^x)) \in \\ &\left\{ \left(\begin{bmatrix} 1 \\ 1 \\ 1 \\ 1 \end{bmatrix}, \begin{bmatrix} 1 \\ 1 \\ 1 \\ 1 \end{bmatrix} \right), \left(\begin{bmatrix} 1 \\ -1 \\ -1 \\ 1 \end{bmatrix}, \begin{bmatrix} 1 \\ -1 \\ -1 \\ 1 \end{bmatrix} \right), \left(\begin{bmatrix} 1 \\ 1 \\ 1 \\ -1 \end{bmatrix}, \begin{bmatrix} 1 \\ 1 \\ 1 \\ 1 \end{bmatrix} \right), \left(\begin{bmatrix} 1 \\ -1 \\ -1 \\ -1 \end{bmatrix}, \begin{bmatrix} 1 \\ -1 \\ -1 \\ 1 \end{bmatrix} \right) \right\}. \end{aligned} \quad (28)$$

We see that some states can change their signs together (x_2 and x_3 in the Example 3) and it will be useful to group these together. To this end, let

$$\mathcal{I}(\Gamma^x) = (\mathbb{I}_1, \dots, \mathbb{I}_{n_\Gamma})$$

where each index set $\mathbb{I}_i \subset \mathbb{Z}_{1, n_x}$ satisfies the following two conditions:

1. $\gamma_j^x = \gamma_k^x$ for all $j, k \in \mathbb{I}_i$ (states indexed by \mathbb{I}_i change sign together).
2. \mathbb{I}_i is maximal (no indices can be added to \mathbb{I}_i without violating the first condition)

This implies that the index sets \mathbb{I}_i are disjoint and hence $\sum_{i=1}^{n_\Gamma} |\mathbb{I}_i| = n_x$. We shall assume that the index sets are ordered in an increasing order, i.e., if $i > j$, then $k > l$ for all $k \in \mathbb{I}_i$ and $l \in \mathbb{I}_j$. This can be achieved without loss of generality by reordering the states. Coming back to Example 3, we get $\mathcal{I}(\Gamma^x) = (\{1\}, \{2, 3\}, \{4\})$.

In order to enforce the symmetry in the Koopman predictor, we will define the groups Γ^z and Γ^v for the lifted vectors $z \in Z$ and $v \in V$. For the input, we use the assumption $\Gamma^v = \Gamma^u$. For defining Γ^z , we need to impose some structure onto the vector z . We do this by fixing the sparsity pattern of the C matrix in order to explicitly link the elements of z with the elements of x . The structure of the matrix C will be block-diagonal

$$C = \text{bdiag}(c_1^\top, \dots, c_{n_x}^\top), \quad (29)$$

where c_i are vectors of user-specified length; the lengths determine how many elements of z will be used for reconstruction of elements of x which can be retrieved as

$$x^i = c_i^\top z^{c_i}, \quad (30)$$

where z^{c_i} is a part of the vector z which corresponds to c_i and has length $|c_i|$. In this work we use $|c_i| = n_z/n_x$, $i = 1 \dots n_x$. The whole vector z can be written as $z = [z^{c_1^\top} \dots z^{c_{n_x}^\top}]^\top$. The set Γ^z is defined as

$$\Gamma^z = \{\text{bdiag}(\gamma_1^x I_{|c_1|}, \dots, \gamma_{n_x}^x I_{|c_{n_x}|}) : \gamma^x \in \Gamma^x\}, \quad (31)$$

so that the elements of γ^x are multiplied with the corresponding parts of z , i.e.,

$$\gamma^z z = \begin{bmatrix} \gamma_1^x I_{|c_1|} & & \\ & \ddots & \\ & & \gamma_{n_x}^x I_{|c_{n_x}|} \end{bmatrix} \begin{bmatrix} z^{c_1} \\ \vdots \\ z^{c_{n_x}} \end{bmatrix} = \begin{bmatrix} \gamma_1^x z^{c_1} \\ \vdots \\ \gamma_{n_x}^x z^{c_{n_x}} \end{bmatrix}. \quad (32)$$

Taking into consideration that some states change signs together ($|\mathbb{I}_i| > 1$ for some i), we can write the same set as

$$\Gamma^z = \left\{ \text{bdiag}(\gamma_{\mathbb{I}_1}^x I_{\nu_1}, \dots, \gamma_{\mathbb{I}_{n_\Gamma}}^x I_{\nu_{n_\Gamma}}) : \gamma^x \in \Gamma^x, \mathbb{I} \in \mathcal{I}(\Gamma^x), \nu_i = \sum_{k \in \mathbb{I}_i} |c_k| \right\}, \quad (33)$$

where $\gamma_{\mathbb{I}_i}^x$ is to be understood as scalar, since all the elements of γ^x have the same value at indices \mathbb{I}_i by definition. The scalars ν_i represent the number of lifted states corresponding to the original states indexed by \mathbb{I}_i , therefore we get $\sum_{i=1}^{n_\Gamma} \nu_i = n_z$. Notice that Γ^z , and therefore h' , depends on the pattern of C which is the connecting element between the vectors x and z . This means that not only the dimension, but also the structure of the lifted space can be tuned in order to obtain good prediction performance.

The matrix A will have a block-diagonal sparsity pattern with the same block sizes as in (33).

$$A = \text{bdiag}(A_1, \dots, A_{n_\Gamma}), \text{ where } A_i \in \mathbb{R}^{\nu_i \times \nu_i} \text{ and } \nu_i = \sum_{k \in \mathcal{I}(\Gamma^x)_i} |c_k|. \quad (34)$$

The matrix $B \in \mathbb{R}^{n_z \times n_u}$ will also have block-diagonal sparsity pattern:

$$B_{i,k} \in \begin{cases} \mathbb{R} & \text{if } h'(\gamma^x)_i = h(\gamma^x)_k \forall \gamma^x \in \Gamma^x \\ 0 & \text{otherwise} \end{cases} \quad (35)$$

where $B_{i,k} = \mathbb{R}$ signifies that the entry is not fixed to zero. Coming back to the Example 3, the predictor would have the structure

$$\begin{aligned} z^+ &= \begin{bmatrix} A_{11} & 0 & 0 & 0 \\ 0 & A_{22} & A_{23} & 0 \\ 0 & A_{32} & A_{33} & 0 \\ 0 & 0 & 0 & A_{44} \end{bmatrix} z + \begin{bmatrix} B_{11} & 0 & 0 \\ 0 & B_{22} & B_{23} \\ 0 & B_{32} & B_{33} \\ 0 & 0 & 0 \end{bmatrix} v \\ \hat{x} &= \begin{bmatrix} c_1^\top & 0 & 0 & 0 \\ 0 & c_2^\top & 0 & 0 \\ 0 & 0 & c_3^\top & 0 \\ 0 & 0 & 0 & c_4^\top \end{bmatrix} z, \end{aligned} \quad (36)$$

where c_i are vectors with user-selected lengths, and $A_{i,j}$ and $B_{i,j}$ are matrices of appropriate sizes.

We say that the LTI system $z^+ = Hz + Gv, x = Fz$ respects the output and input symmetries γ^x and γ^v respectively, if for every trajectory of the LTI system $(z_t^a, x_t^a, u_t^a)_{t=0}^\infty$, there exists a sequence $(z_t^b)_{t=0}^\infty$ such that $(z_t^b, \gamma^x x_t^a, \gamma^u u_t^a)_{t=0}^\infty$ is also its trajectory.

Lemma 1. *Assume an observable LTI system $z^+ = Hz + Gv, x = Fz$, where the output x and input u respect the symmetries Γ^x and Γ^v . The system can be transformed into an equivalent form, which has the same output x , its state respects the symmetry Γ^z , and its state matrices have the block-diagonal form introduced above.*

Proof. We can assume that the original system (H, G, F) has been transformed into its observer form $(\hat{A}, \hat{B}, \hat{C})$ [29, Section 6.4.2] and its states have been reordered such that

$$\hat{C} = \begin{bmatrix} 1 & 0 & \dots & 0 & 0 & \dots & 0 \\ \times & 1 & \dots & 0 & 0 & \dots & 0 \\ & & \ddots & & 0 & \dots & 0 \\ \times & \times & \dots & 1 & 0 & \dots & 0 \end{bmatrix}, \quad (37)$$

where \times are unfixed entries. We want to find a full-rank matrix T to perform the similarity transformation

$$A = T^{-1} \hat{A} T \quad (38a)$$

$$B = T^{-1} \hat{B} \quad (38b)$$

$$C = \hat{C} T, \quad (38c)$$

with C having the block-diagonal structure used in (29). We can write $C = \hat{C} T$ as

$$\begin{bmatrix} c_1^\top & 0 & 0 & 0 \\ 0 & c_2^\top & 0 & 0 \\ 0 & 0 & \ddots & 0 \\ 0 & 0 & 0 & c_{n_x}^\top \end{bmatrix} = \begin{bmatrix} 1 & 0 & 0 & 0 & 0 & \dots & 0 \\ \hat{c}_{2,1} & 1 & 0 & 0 & 0 & \dots & 0 \\ \vdots & & \ddots & & 0 & \dots & 0 \\ \hat{c}_{n_x,1:(n_x-1)} & & & 1 & 0 & \dots & 0 \end{bmatrix} \underbrace{\begin{bmatrix} c_1^\top & 0 & 0 & 0 \\ T_{2,1} & c_2^\top & 0 & 0 \\ \vdots & & \ddots & 0 \\ T_{n_x,1} & T_{n_x,2} & \dots & c_{n_x}^\top \end{bmatrix}}_{T_F} \quad (39)$$

where $T_{i,j}$ is a row block of length $|c_i|$ such that

$$T_{i,j} = \begin{cases} -\sum_{k=1}^{i-1} \hat{c}_{i,k} T_{k,j}, & \text{if } i > j \\ c_i^\top, & \text{if } i = j \\ 0, & \text{if } i < j. \end{cases} \quad (40)$$

The first n_x rows of T will have full row rank with this construction, since the observability assumption implies $c_i \neq \mathbf{0}_{|c_i|}$. The remainder (matrix T_F) is multiplied by 0 in the matrix \tilde{C} , therefore it can be freely chosen such that T has full rank.

We shall demonstrate the construction of T on a simple example with $n_y = 3, n_z = 6$, and $c_1 = [1, 2], c_2 = [3, 0], c_3 = [5, 6]$. The equation (39) is then

$$\begin{bmatrix} 1 & 2 & 0 & 0 & 0 & 0 \\ 0 & 0 & 3 & 0 & 0 & 0 \\ 0 & 0 & 0 & 0 & 5 & 6 \end{bmatrix} = \begin{bmatrix} 1 & 0 & 0 & 0 & 0 & 0 \\ a & 1 & 0 & 0 & 0 & 0 \\ b & c & 1 & 0 & 0 & 0 \end{bmatrix} \left[\frac{\begin{bmatrix} 1 & 2 & 0 & 0 & 0 & 0 \\ -a & -2a & 3 & 0 & 0 & 0 \\ ac-b & 2(ac-b) & -3c & 0 & 5 & 6 \end{bmatrix}}{T_F} \right]. \quad (41)$$

We see that the matrix T has full rank (provided T_F has full row rank) for all values of the unfixed entries.

Having the matrix C in the block-diagonal form, we will use the definition of Γ^z (33) and the sparsity patterns of A (34) and B (35) to show that

$$A(\gamma^z z) + B(\gamma^v v) = \gamma^z (Az + Bv) \quad \forall \Gamma^x, \quad (42)$$

where $\gamma^x \in \Gamma^x$, $\gamma^v = h(\gamma^x)$, and $\gamma^z = h'(\gamma^x)$. The equation can be separated into two conditions

$$A\gamma^z = \gamma^z A, \quad (43)$$

and

$$B\gamma^v = \gamma^z B. \quad (44)$$

The equation (43) is a product of two block-diagonal matrices with the same block structure with the definitions (33) and (34). Block-diagonal matrices commute if and only if their blocks commute and since the blocks of γ^z are scalar matrices, they commute with every matrix and therefore (43) holds.

The second equation (44) can be written as

$$\left[\begin{array}{c|c|c|c} \gamma_1^v & \gamma_2^v & \dots & \gamma_{n_v}^v \\ \hline \end{array} \right] \odot B - \left[\begin{array}{c|c|c} \gamma_1^z & & \\ \gamma_2^z & & \\ \vdots & & \\ \gamma_{n_z}^z & & \\ \hline \end{array} \right] \odot B = 0, \quad (45)$$

after factoring out B , we obtain

$$\left(\left[\begin{array}{c|c|c|c} \gamma_1^v & \gamma_2^v & \dots & \gamma_{n_v}^v \\ \hline \end{array} \right] - \left[\begin{array}{c|c|c} \gamma_1^z & & \\ \gamma_2^z & & \\ \vdots & & \\ \gamma_{n_z}^z & & \\ \hline \end{array} \right] \right) \odot B = 0. \quad (46)$$

Let us call the matrix in parentheses D and obtain

$$D \odot B = 0. \quad (47)$$

The matrix D will be 0 only in places, where the elements of γ^v and γ^z are equal

$$\gamma_k^z = \gamma_p^v \implies D_{k,p} = 0 \text{ such that } \gamma^v = h(\gamma^x), \gamma^z = h'(\gamma^x), \forall \gamma^x \in \Gamma^x. \quad (48)$$

It is on these indices where the matrix B can have nonzero entries, it has to be zero everywhere else in order for (47) to hold. We see from (35) that the matrix B fulfills this condition by definition.

Let us show an example with $n_u = 2$, $n_z = 3$, $\gamma^z = [1, s, s]^\top$ and $\gamma^v = [1, s]^\top$, where $s \in \{-1, 1\}$.

$$\begin{bmatrix} b_1 & b_2 \\ b_3 & b_4 \\ b_5 & b_6 \end{bmatrix} \begin{bmatrix} 1 & 0 \\ 0 & s \end{bmatrix} = \begin{bmatrix} 1 & 0 & 0 \\ 0 & s & 0 \\ 0 & 0 & s \end{bmatrix} \begin{bmatrix} b_1 & b_2 \\ b_3 & b_4 \\ b_5 & b_6 \end{bmatrix} \quad (49)$$

$$\begin{bmatrix} \mathbf{b}_1 & sb_2 \\ b_3 & \mathbf{sb}_4 \\ b_5 & \mathbf{sb}_6 \end{bmatrix} = \begin{bmatrix} \mathbf{b}_1 & b_2 \\ sb_3 & \mathbf{sb}_4 \\ sb_5 & \mathbf{sb}_6 \end{bmatrix}. \quad (50)$$

The bold elements have the same value for all s , we see that b_2, b_3 , and b_5 have to be zero in order for the equation to hold. The matrix B will then be

$$B = \begin{bmatrix} b_1 & 0 \\ 0 & b_4 \\ 0 & b_6 \end{bmatrix}. \quad (51)$$

□

Corollary 1. Assume a nonlinear system $x^+ = f(x, u)$, its predictor $z^+ = Az + Bv$, $\hat{x} = Cz$ both with symmetry Γ^x according to (24) and (25), and symmetric lifting functions Φ and Ψ such that $\gamma^z \Phi(x) = \Phi(\gamma^x x)$ and $\gamma^v \Psi(u) = \Psi(\gamma^u u)$, where $\gamma^x \in \Gamma^x$, $\gamma^v = \gamma^u = h(\gamma^x)$, and $\gamma^z = h'(\gamma^x)$.

If $(\hat{x}_t)_{t=0}^\infty$ and $(\widehat{\gamma^x x})_{t=0}^\infty$ are predictions of the symmetrical trajectories $(x_t)_{t=0}^\infty$ and $(\gamma^x x_t)_{t=0}^\infty$ respectively, then $(\widehat{\gamma^x x})_{t=0}^\infty$ is equal to symmetrized $(\hat{x}_t)_{t=0}^\infty$, i.e. $(\widehat{\gamma^x x})_{t=0}^\infty = (\gamma^x \hat{x}_t)_{t=0}^\infty$, achieving the same prediction error as $(\hat{x}_t)_{t=0}^\infty$ achieves for predicting $(x_t)_{t=0}^\infty$.

Proof. Let us have a nonlinear system (1) with symmetries (24). The symmetrical states $x_t, \gamma x_t$ of the system are obtained as

$$\begin{aligned} x_t &= S_f^t(x_0, (u_0, \dots, u_{t-1})) \\ \gamma^x x_t &= S_f^t(\gamma^x x_0, (\gamma^u u_0, \dots, \gamma^u u_{t-1})), \end{aligned} \quad (52)$$

where S_f^t denotes the flow of the system f up to time t with initial condition x_0 and input sequence u_0, \dots, u_{t-1} . Using the same initial state and inputs, the lifted states $z_t, \gamma^z z_t$ of the LTI predictor (A, B) are

$$\begin{aligned} z_t &= S_{A,B}^t(\Phi(x_0), (\Psi(u_0), \dots, \Psi(u_{t-1}))) \\ \gamma^z z_t &= S_{A,B}^t(\gamma^z \Phi(x_0), (\gamma^v \Psi(u_0), \dots, \gamma^v \Psi(u_{t-1}))). \end{aligned} \quad (53)$$

The prediction of x is obtained as $\hat{x} = Cz$, therefore

$$\begin{aligned} \hat{x}_t &= C \cdot S_{A,B}^t(\Phi(x_0), (\Psi(u_0), \dots, \Psi(u_{t-1}))) \\ \widehat{\gamma^x x}_t &= C \cdot S_{A,B}^t(\Phi(\gamma^x x_0), (\Psi(\gamma^u u_0), \dots, \Psi(\gamma^u u_{t-1}))). \end{aligned} \quad (54)$$

Using the symmetries of the lifting functions and definition of γ^z (32), we can rewrite the second equation as

$$\begin{aligned} \widehat{\gamma^x x}_t &= C \cdot S_{A,B}^t(\gamma^z \Phi(x_0), (\gamma^u \Psi(u_0), \dots, \gamma^u \Psi(u_{t-1}))) \\ &= C \gamma^z z_t \\ &= \gamma^x C z_t \\ &= \gamma^x \hat{x}_t. \end{aligned} \quad (55)$$

□

Symmetric lifting functions The definition of Φ from (19) can be extended to respect the symmetries by simply defining it on a symmetric dataset

$$\bar{z}_0^i = \Phi(\bar{x}_0^i) \quad \forall i \in \mathbb{Z}_{1,2^{n_\Gamma} \cdot N}, \quad (56)$$

where

$$(\bar{x}_0^i, \bar{z}_0^i) \in \{(\gamma^x x, \gamma^z z) : \gamma^z = h(\gamma^x) \quad \forall \gamma^x \in \Gamma^x\} \quad (57)$$

Since the input transformation Ψ is done channel-wise, for each Ψ_k we can simply add the cost

$$\sum_{j \in \mathbb{Z}_{1,q_k}} \sum_{u_k^j \in U_k, v_k^j \in V_k} \|\gamma^v v_k^j - \Psi_k(\gamma^u u_k^j)\|_2^2 \quad (58)$$

to the regularizations $\theta(\cdot)$ in (23).

5 Implementation details

This section describes certain details concerning the problem (23). First, we address the trajectory preparation in Section 5.1. Solving of the problem (23) and its initialization are discussed in Sections 5.2 and 5.3 respectively.

A summary of the whole process from data preparation to solving (23) is provided in the Section 5.4.

5.1 Trajectory preparation

In order to improve the prediction capabilities and restrict overfitting, we force consecutive trajectories to have the same lifted values in their endpoints. This *endpoint consistency* is enforced by the term $\sum_{(a,b) \in \mathcal{S}} \|z_{H_T}^a - z_0^b\|_2^2$ of (23). The effect of (not) using it is shown in the Fig.2. In our examples, we enforce the endpoint consistency and the prediction capabilities of the predictor exceed the learning horizon H_T . This is shown in the Fig.14 in the numerical examples section.

To make sure that our dataset contains consecutive trajectories, we generate long trajectories of length rH_T and split each into r trajectories of length H_T . Hence the final state of the first trajectory is the initial state of the second one and so on (only the last trajectories will have “free” final states x_{rH_T}). The indices of consecutive trajectories are stored in the set \mathcal{S} , as depicted in the Fig.3.

Since the problem (23) is very flexible in terms of free variables, we need to make a clear distinction between controlled and autonomous trajectories, to prevent overfitting (we do not want controlled trajectory to be approximated by autonomous response and vice versa). For this, it is sufficient to start two trajectories from the same initial state, with different control inputs. This is also depicted in Fig.3. We state this formally in the following Lemma.

Lemma 2. *Assume that we have two distinct trajectories of the nonlinear system (1), \mathcal{T}_i and \mathcal{T}_j , with $x_0^i = x_0^j$, $u_0^i \neq u_0^j$, and $y_1^i \neq y_1^j$. For any Koopman predictor \mathcal{K} , which approximates the trajectories with zero error, such that $z_0^i = z_0^j$, $z_0^i = \Phi(x_0^i)$, $z_0^j = \Phi(x_0^j)$, $Cz_1^i = y_1^i$, $Cz_1^j = y_1^j$, it holds that $\Psi(u_0^i) \neq \Psi(u_0^j)$.*

Proof. Let us have two trajectories

$$\begin{aligned} \mathcal{T}_i &: (x_0^i, y_0^i, u_0^i), (y_1^i) \\ \mathcal{T}_j &: (x_0^j, y_0^j, u_0^j), (y_1^j) \end{aligned} \quad (59)$$

such that $i \neq j$, $u_0^i \neq u_0^j$, and $y_1^i \neq y_1^j$. We want to show that if $x_0^i = x_0^j$ then $\Psi(u_0^i) \neq \Psi(u_0^j)$.

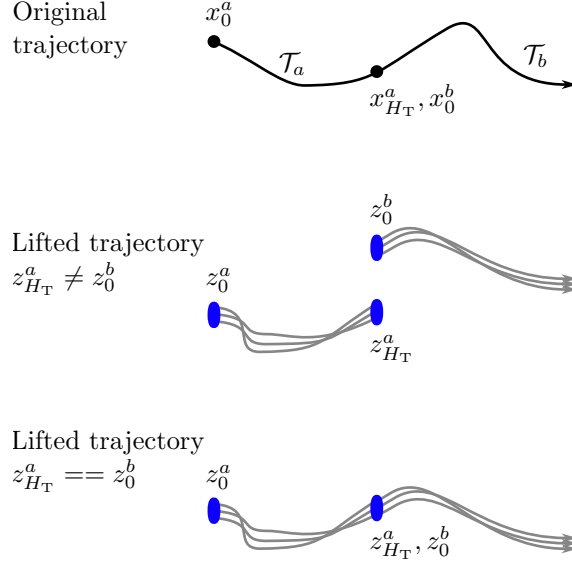


Figure 2: This figure demonstrates the effect of enforcing the endpoint consistency. Note that even when not enforcing it, we still obtain a valid predictor although the prediction capabilities will be strictly limited to the learning horizon H_T .

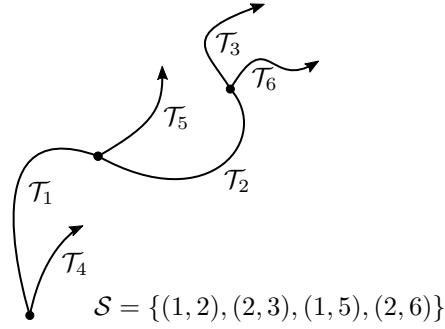


Figure 3: Example of trajectories used for learning and their interconnections. We see that one long trajectory was split into $\mathcal{T}_1, \mathcal{T}_2$, and \mathcal{T}_3 . The trajectories $\mathcal{T}_{4,5,6}$ start from the same initial conditions as $\mathcal{T}_{1,2,3}$ in this order. The set \mathcal{S} contains the indices of the interconnected trajectories, denoting that the pairs of connected trajectories are $(\mathcal{T}_1, \mathcal{T}_2), (\mathcal{T}_2, \mathcal{T}_3)$, etc.

Let us write the predictions of the Koopman predictor

$$\begin{aligned} \hat{y}_1^i &= C(Az_0^i + Bv_0^i) \\ \hat{y}_1^j &= C(Az_0^j + Bv_0^j), \end{aligned} \tag{60}$$

where $z_0^i = \Phi(x_0^i)$, $z_0^j = \Phi(x_0^j)$, $v_0^i = \Psi(u_0^i)$, $v_0^j = \Psi(u_0^j)$. By subtracting them, we obtain

$$\hat{y}_1^i - \hat{y}_1^j = CA(z_0^i - z_0^j) + CB(v_0^i - v_0^j). \tag{61}$$

Knowing that we have zero approximation error, we can write $\hat{y}_1^i = y_1^i$ and $\hat{y}_1^j = y_1^j$. Then by using

the inequality $y_1^i \neq y_1^j$, we get

$$CA(z_0^i - z_0^j) + CB(v_0^i - v_0^j) \neq 0. \quad (62)$$

The inequality can be fulfilled by either the initial states or the inputs not being equal. However, if both trajectories start from the same initial condition, we get $z_0^i = z_0^j$ and the inequality can be only satisfied by $v_0^i \neq v_0^j$. \square

5.2 Solving the Koopman optimization problem

The problem (23) can be formulated as a nonlinear unconstrained optimization problem after elimination of the linear equality constraints. It can be solved by a variety of solvers; in our case, we use the ADAM [17] optimization algorithm. ADAM is a first-order method for unconstrained problems, therefore it requires gradients of the cost function. We calculate the gradients of (23), via automatic differentiation (AD) routines, specifically by the packages Flux [16],[15] and Zygote [14] from Julia [6].

We would like to note that it seems beneficial to fix the values V_k during the first iterations of the ADAM solver. The lifted inputs will be more likely to retain the physical meaning of the original input variables. This is demonstrated in our last example in the Figures 15 and 16. In this paper, we fixed the input for the first 500 iterations.

5.3 Initialization values

The variables of (23) need to be initialized. Table 1 lists the choices used in this paper. We use $\mathcal{U}_{\alpha,\beta}$ to denote uniform distribution in the interval $[\alpha, \beta]$.

Variable	Initialization value(s)
z_0^i	Each element from $\mathcal{U}_{-1/2,1/2}$
V_k	Same as U_k
A	$a_{i,j} \in \mathcal{U}_{-1/2,1/2}$
B	$b_{i,j} \in \mathcal{U}_{-1/2,1/2}$
C	$c_{i,j} \in \mathcal{U}_{-1/2,1/2}$

Table 1: Initialization values for the problem (23).

It might be beneficial in some cases to initialize A such that its spectral radius is less than 1, which will make the initialized system (A, B, C) stable from a control-systems point of view.

5.4 Summary: Learning Koopman predictor

The algorithm 1 summarizes the procedure for learning the Koopman predictor.

Algorithm 1 Find the Koopman predictor (A,B,C,Φ, Ψ)

Input: f, g, X_0, H_T, q_k, N

- 1: Identify symmetries of the system f, g according to 4 and create the sparsity patterns for A, B, C .
- 2: Choose the number of quantization levels q_k and create the quantized channels U_k .
- 3: Generate N trajectories \mathcal{T}_i of length H_T according to 5.1
- 4: Initialize the matrices A, B, C , and the elements of Z_0 and V_k according to 5.3.
- 5: Solve (23), optionally fix the values V_k as mentioned in 5.2.

Output: A, B, C, Z_0, V_k

6 Koopman operator in control

In this section, we shall demonstrate the advantage of using a Koopman operator in control applications. More specifically, we will consider a Model Predictive Control (MPC) [24]. For a general nonlinear system (1), the MPC can be formulated as

$$\begin{aligned}
 J^* = \min \quad & \sum_{t=1}^H J_n(x_t) + J_c(x_t) \\
 \text{s.t.} \quad & x_{t+1} = f(x_t, u_t) \\
 & x_t \in X \\
 & u_t \in U,
 \end{aligned} \tag{63}$$

where J_c and J_n are convex and non-convex parts of the cost function in this order. This problem is non-convex due to the function J_n and the generally nonlinear constraint $x_{t+1} = f(x_t, u_t)$; this makes the problem difficult to solve in general. We can, however, use the Koopman methodology to reformulate the problem in a convex fashion. We can eliminate the non-convex cost $J_n(x_t)$ by setting it as an additional output $\chi_t = J_n(x_t)$ and use the Koopman predictor of the form

$$\begin{aligned}
 z_{t+1} &= Az_t + Bv_t \\
 \begin{bmatrix} \hat{\chi}_t \\ \hat{x}_t \end{bmatrix} &= Cz_t \\
 z_0 &= \Phi(x_0),
 \end{aligned} \tag{64}$$

where $\hat{\chi}_t$ is an approximation of the non-convex cost $\chi_t = J_n(x_t)$. We can now rewrite (63) as

$$\begin{aligned}
 \hat{J}^* = \min \quad & \sum_{t=1}^H \hat{\chi}_t + J_c(\hat{x}_t) \\
 \text{s.t.} \quad & z_{t+1} = Az_t + Bv_t \\
 & \begin{bmatrix} \hat{\chi}_t \\ \hat{x}_t \end{bmatrix} = Cz_t \\
 & z_0 = \Phi(x_0) \\
 & \hat{x}_t \in X \\
 & v_t \in V,
 \end{aligned} \tag{65}$$

where X is assumed to be convex and V is a box-constraint by construction (due to the channel-wise lifting). Under these assumptions, the problem (65) is convex.

In a wide range of applications, the convex part of the cost is quadratic and the constraints are upper and lower bounds on some of the variables. This allows the user to formulate the problem ((65))

as a convex Quadratic Program (QP) – a well-studied class of convex optimization problems with many solvers tailored to solving them efficiently such as ProxSuite [5], OSQP [32], and COSMO [12].

6.1 Koopman MPC

Let us exploit the benefits of the QP formulation and formulate our problem concretely, in a tracking form (minimizing the deviation of y_t from known y_{ref}) consistent with our own implementation used later in the Section 8. We shall refer to this optimization problem as Koopman MPC (KMPC):

$$\begin{aligned}
\min_{\Delta v_t, z_t} \quad & \sum_{t=1}^H \|y_{\text{ref}} - Cz_t\|_Q^2 + \|v_t\|_R^2 + \|\Delta v_t\|_{R_d}^2 \\
\text{s.t.} \quad & z_{t+1} = Az_t + Bv_t & t = 1 \dots H-1 \\
& v_t = \Delta v_t + v_{t-1} & t = 0 \dots H \\
& y_{\text{low}} \leq y_t \leq y_{\text{up}} & t = 1 \dots H \\
& v_{\text{low}} \leq v_t \leq v_{\text{up}} & t = 1 \dots H \\
& \Delta v_{\text{low}} \leq \Delta v_t \leq \Delta v_{\text{up}} & t = 1 \dots H \\
& z_0 = \hat{\Phi}(x_0) \\
& v_0 = \Psi(u_{\text{prev}}),
\end{aligned} \tag{66}$$

where $y_t = \begin{bmatrix} \hat{\chi}_t \\ \hat{x}_t \end{bmatrix}$, $Q \succcurlyeq 0$, $R \succ 0$, and $R_d \succ 0$. As mentioned before, this formulation solves the tracking problem where y_{ref} is an external parameter, and Δv_t is the optimization variable (instead of v_t). The output, input, and input rate constraints are the pairs $(y_{\text{low}}, y_{\text{up}})$, $(v_{\text{low}}, v_{\text{up}})$, and $(\Delta v_{\text{low}}, \Delta v_{\text{up}})$ in this order.

The optimal solution is recovered as $u_t^* = \hat{\Psi}^{-1}(v_t^*)$, where $\hat{\Psi}$ is linearly interpolated version of Ψ which is discussed in detail the following Section. The problem is solved repeatedly at each time step, always using only the first control input u_1^* and then recalculating the solution from a new initial state. This approach provides closed-loop control and can be seen in Fig. 4.

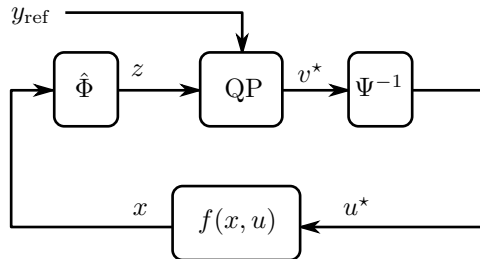


Figure 4: General MPC scheme using the Koopman operator as a control design model.

6.2 Control-related considerations

For use in control, we need to expand the domain of the lifting function Φ (19) to X , instead of X_0 . Another matter to consider is the invertibility of Ψ (21), since it is not guaranteed from (23).

Both of these matters are addressed in the following sections 6.2.3 and 6.2.4.

Regarding the connection of the Koopman predictor and MPC, we can expect the lifting functions to have a non-zero lifting error since we are working only with an approximation of the Koopman

operator. The lifting error can be calculated and its knowledge exploited as a part of the MPC algorithm. This option is addressed in 6.2.1.

The last consideration is setting of the lifted input rate bounds $\Delta v_{\text{up/low}}$. These bounds do not naturally arise by finding the lifting functions (unlike $v_{\text{up/low}}$) and need to be set manually. We address this further in 6.2.2.

Lastly, we note that the problem (66) has the lifted state vectors z_t as variables. This greatly increases the total number of optimization variables since the dimension n_z may be large (recall that we are approximating infinite-dimensional operator). In the appendix, we show that the MPC can be formulated in a so-called condensed formulation, which has only Δv_t as variables, reducing the computational burden.

6.2.1 Lifting error

When the lifting via $\hat{\Phi}$ is not exact, we can use the knowledge of $\hat{\Phi}$ to calculate the lifting error at x_{init} and set it as output disturbance to the MPC to increase the precision of the calculation for the first timestep. The augmented output equation then reads

$$y_t = Cz_t + d_t, \quad (67)$$

where d is the initial-state lifting error

$$d_t = g(x_{\text{init}}) - C\hat{\Phi}(x_{\text{init}}) \quad \forall t = 1, \dots, H. \quad (68)$$

This can be easily implemented by augmenting the state-space model as

$$\bar{A} = \begin{bmatrix} A & \\ & \zeta I \end{bmatrix}, \bar{B} = \begin{bmatrix} B \\ 0 \end{bmatrix}, C = [C \quad I], \quad (69)$$

where $|\zeta| \leq 1$ is the decay rate of d . Constant disturbance model is achieved by setting $\zeta = 1$.

The error could be also estimated for the whole prediction horizon iteratively, by solving the QP multiple times and evaluating (68) for all the states x_t .

6.2.2 Input rate bounds

The bounds on Δv are not trivial to choose because the lifted-space bounds on v will not correspond to the real bounds on u because of the nonlinearity of Ψ , as seen in Fig.5. Possible solutions are

1. use the bounds with soft constraints to make them flexible
2. use ideas from nonlinear MPC and make an iterative scheme (i.e. solve the QP multiple times while iteratively adjusting the bounds.)
3. use linearization of Ψ to set the bound
4. set the bounds on Δv conservatively, so that the worst case of Δu is guaranteed to be within its bounds.

6.2.3 Interpolation of Φ

As a result of the optimization process, we will obtain the samples of the function Φ in the form of pairs (x_0^i, z_0^i) , instead of the function itself. One needs to approximate $\hat{\Phi}$ by interpolation as

$$\hat{\Phi}(x, p) = h(X_0, Z_0, x, p), \quad (70)$$

where h is an interpolation method with parameters p , e.g., the K-Nearest Neighbours (k-NN). The question is how to choose the parameters p ? One way would be to simply evaluate the lifting error across all datapoints and select the best one as

$$p^* = \operatorname{argmin}_{p \in P} \sum_{x \in X_0} \|g(x) - C\hat{\Phi}(x, p)\|_Q^2, \quad (71)$$

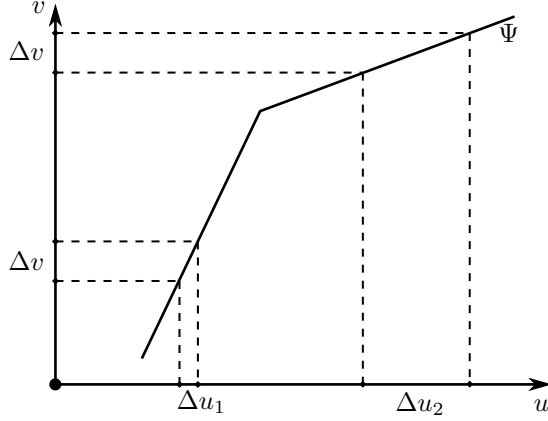


Figure 5: Example of a function Ψ , which would pose challenges with identifying the desired bounds on Δv . We see that constant Δv can correspond to both Δu_1 and Δu_2 depending on the current value of the input.

where P is the parameter space. We use the $\|\cdot\|_Q$ norm to make the weighting consistent with the KMPC cost function in (66). Another possibility is to adapt the interpolation scheme dynamically to the current initial point x_{init} of the MPC as

$$p^* = \operatorname{argmin}_{p \in P} \|g(x_{\text{init}}) - C\hat{\Phi}(x_{\text{init}}, p)\|_Q^2. \quad (72)$$

Doing this would ensure the precision of the first few steps of the prediction, as well as the precision of the first control input, which is used for the closed-loop control. The tradeoff is that every iterate of the closed-loop would involve searching for the best interpolation parameters either via solving an optimization problem, or simply by evaluating the lifting function $|P|$ times (if the search space P is finite, such as for k-NN).

6.2.4 Invertibility of Ψ

The function Ψ might be required to be invertible if we intent to use its continuous interpolation in the MPC.

In order to ensure this, we can either manually limit the domain of each channel to its invertible parts, which boils down to manually limiting the domain of n_u scalar functions of one variable.

Another option is enforcing monotonicity of individual Ψ_k by adding the following regularization as the additional cost term $\theta(\cdot)$ in (23):

$$\left\| \left| v_k^{q_k} - v_k^1 \right| - \sum_{i=1}^{q_k-1} |v_k^{i+1} - v_k^i| \right\|_2^2, \quad (73)$$

where v_k are samples of Ψ_k . The cost (73) is explained in the following Lemma.

Lemma 3. *A sequence of q_k consecutive samples $[v_k^1, \dots, v_k^{q_k}]$ is monotonous if and only if*

$$|v_k^{q_k} - v_k^1| = \sum_{i=1}^{q_k-1} |v_k^{i+1} - v_k^i|. \quad (74)$$

Proof. The final element of the sequence can be written as

$$v_k^{q_k} = v_k^1 + \sum_{i=1}^{q_k-1} \epsilon_i, \quad (75)$$

where $\epsilon_i = v_k^{i+1} - v_k^i$. We reorganize the terms

$$v_k^{q_k} - v_k^1 = \sum_{i=1}^{q_k-1} \epsilon_i \quad (76)$$

and put both sides of the equation in absolute value

$$|v_k^{q_k} - v_k^1| = \left| \sum_{i=1}^{q_k-1} \epsilon_i \right|. \quad (77)$$

If the function is monotonous, all the ϵ_i have the same sign and hence

$$\left| \sum_{i=1}^{q_k-1} \epsilon_i \right| = \sum_{i=1}^{q_k-1} |\epsilon_i|. \quad (78)$$

Finally, by assuming the monotonicity of Ψ_k , we can put (77) and (78) together and we obtain

$$|v_k^{q_k} - v_k^1| = \sum_{i=1}^{q_k-1} |\epsilon_i| = \sum_{i=1}^{q_k-1} |v_k^{i+1} - v_k^i|. \quad (79)$$

Therefore, if the sequence v_k^i is monotonous, the equality (74) must hold.

Let us now prove the other direction. We claim that if (74) holds, then the function is monotonous. In the simple cases where the terms inside the absolute values are either all non-negative or non-positive, it is trivial to see that the function will be non-decreasing or non-increasing respectively.

The interesting case is where the signs are different. Let us assume, without loss of generality, that $v^2 - v^1 \leq 0$, and all the other terms are nonnegative. If we rewrite (79) without the absolute values, we obtain

$$(v_k^1 - v_k^2) + (v_k^3 - v_k^2) + (v_k^4 - v_k^3) + \dots + (v_k^{q_k} - v_k^{q_k-1}) = v_k^{q_k} - v_k^1. \quad (80)$$

It is clear that

$$v_k^1 - v_k^2 = 0, \quad (81)$$

therefore Ψ_k will be monotonically non-decreasing. The same approach can be used for multiple sign changes, which concludes the proof. \square

7 Summary: Koopman MPC

The algorithm 2 summarizes the procedure for designing the KMPC.

The algorithm 3 shows the usage of KMPC in closed loop. The step 6 is equivalent to applying the control inputs to the real system.

Algorithm 2 Create the Koopman MPC

Input: $A, B, C, Z_0, V_k, H, Q, R, R_d$

- 1: Create interpolated lifting function $\hat{\Phi}$ according to 6.2.3.
- 2: Decide on the strategy for inverting Ψ as in 6.2.4, optionally include the cost (73) into the term $\theta(\cdot)$ in (23).
- 3: Decide on the strategy for dealing with the input rate bounds, if applicable, according to 6.2.2.
- 4: Formulate the KMPC, either in the sparse (66) or the dense (104) formulation.

Output: function $\text{KMPC}(y_{\text{ref}}, x_0, u_{\text{prev}}) \rightarrow v^*$

Algorithm 3 Closed loop KMPC

Input: $y_{\text{ref}}, \text{KMPC}$

- 1: Initialization: $u_{\text{prev}} \leftarrow 0, x_0 = x_{\text{init}}$
 - 2: **while** true **do**
 - 3: $z_0 \leftarrow \hat{\Phi}(x_0)$.
 - 4: $v_0^* \leftarrow \text{KMPC}(y_{\text{ref}}, x_0, u_{\text{prev}})$ [Problem (66)]
 - 5: $u_0^* \leftarrow \hat{\Psi}^{-1}(v_0^*)$
 - 6: $x_0 \leftarrow f(x_0, u_0^*)$
 - 7: $u_{\text{prev}} \leftarrow u_0^*$
 - 8: Wait for the next timestep.
 - 9: **end while**
-

8 Numerical examples

In this section, we shall demonstrate the following properties of our approach:

1. discovering discontinuous lifting functions
2. finding exact lift even for systems with multiple equilibria
3. controlling systems with multiple equilibria
4. controlling systems with nonlinear input functions
5. control of realistic, highly nonlinear systems which are difficult to control with standard methods of control.

The first two properties are demonstrated in the first example, on a system with known analytical solution. The discontinuous lifting is of particular interest, since a lot of current methods (such as EDMD and its derivatives) require the prior knowledge (or guess) of the lifting function(s) Φ . In order to find the Koopman operator using these methods, we would need to know whether its lifting functions are discontinuous (along with the particular type and location of discontinuity). This is not required by our method.

The second example shows the control of a system with multiple equilibria, using the KMPC, we compare our method to EDMD [21] and Optimal eigenfunction [22].

The third example shows control of a system that cannot be controlled by other Koopman methods which do not have nonlinear input transformation.

The last example is of a more practical nature; it shows that our approach can be used to synthesize a single controller that can drive the vehicle in normal conditions as well as to stabilize it from an unstable state. Vehicles are highly nonlinear systems, especially when the wheels lose grip with the road. Therefore such maneuvers are rather challenging, since they require exploitation of the nonlinear dynamics of the vehicle. We compare both maneuvers against MPC based on local linearization (LMPC) and a Nonlinear MPC (NMPC).

8.1 Discontinuous lifting with multiple equilibria

This example demonstrates that our algorithm can find discontinuous lifting functions and systems with multiple equilibria. We will use the system from [4], to which the analytical solution is known. We empirically show that our algorithm converges to the analytical solution from any initial condition of the ADAM solver.

Consider the nonlinear system

$$\begin{aligned} \dot{x} &= f(x) \\ f(x) &= \begin{cases} -(x-1) & \text{if } x > 0 \\ 0 & \text{if } x = 0 \\ -(x+1) & \text{if } x < 0 \end{cases} \end{aligned} \quad (82)$$

The corresponding Koopman operator derived in [4] is of the form

$$\dot{z} = Az, y = Cz, \quad (83)$$

where

$$\begin{aligned} A &= \begin{bmatrix} -1 & 1 \\ 0 & 0 \end{bmatrix} \\ C &= [1 \quad 1]. \end{aligned} \quad (84)$$

The output $y = z_1 + z_2$ is equal to the nonlinear state x . The eigenvalues and eigenfunctions of the operator (84) are

$$\begin{aligned} \lambda_1 &= -1, & \Phi_1 &= x - \text{sign}(x), \\ \lambda_2 &= 0, & \Phi_2 &= \text{sign}(x). \end{aligned} \quad (85)$$

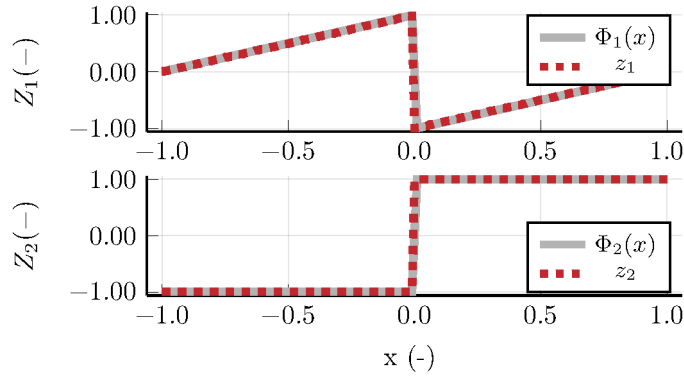


Figure 6: Comparison of analytical and learned lifted function of the one-dimensional system with multiple isolated points. We use z_1 and z_2 to denote the first and second coordinate of the lifted space.

In order to learn the Koopman predictor, we have generated 300 trajectories of the system (82) of length $H_T = 20$ which were sampled with $T_s = 0.1s$. Using the approach 1, we obtained

a discrete-time Koopman predictor (\hat{A}_d, \hat{C}_d) , which was transformed into a continuous system by $(\hat{A}, \hat{C}) = (\frac{\log(\hat{A}_d)}{T_s}, \hat{C}_d)$. To compare our result with the analytical solution (84), we transformed both the analytical system (A, C) and the learned approximation (\hat{A}, \hat{C}) into observer canonical form

$$A_o = \begin{bmatrix} 0 & 1 \\ 0 & -1 \end{bmatrix}, \quad C_o = [1 \quad 0],$$

$$\hat{A}_o = \begin{bmatrix} -0.0003 & 1.0508 \\ 0.005 & -0.9989 \end{bmatrix}, \hat{C}_o = [1 \quad 0].$$

We can see that the approximated system is numerically close to the analytical solution. The continuous eigenvalues of learned Koopman system were $\hat{\lambda}_{1,2} = [-1.004 \quad 0.005]$. The estimated eigenfunctions are compared to the real ones in Fig.6.

We compare the open-loop prediction capabilities of our method with EDMD of different orders n_z in Fig.7. The basis functions for the EDMD were thin plate spline radial basis functions

$$\Phi_{\text{rbf}}(x) = \|x - x_c\|^2 \log(\|x - x_c\|), \quad (86)$$

with centers x_c selected randomly from the interval $[-1, 1]$. We can see that the proposed method provides more precision than EDMD while having only two lifted states.

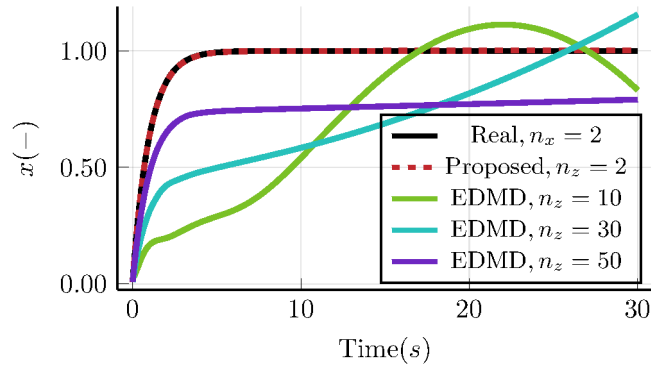


Figure 7: Open-loop predictions of our method and EDMD of different orders. The initial state of the trajectories was $x_0 = 0.01$, close to the unstable equilibrium at $x_e = 0$. The proposed predictor has the lowest order and the highest precision due to the precise identification of the discontinuous lifting functions.

To test convergence of our algorithm, we learned 100 Koopman predictors with different initial conditions of the ADAM solver generated according to 1. The eigenvalues converged to the analytical result in all cases. The results can be seen in Fig.8.

We can see that our approach was able to discover discontinuous eigenfunctions and system with multiple equilibria without any prior information.

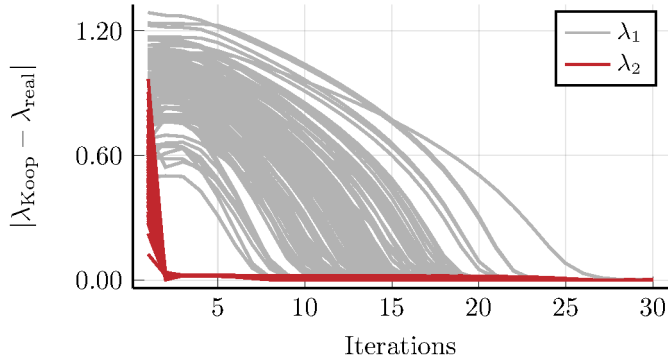


Figure 8: Evolution of the error of the continuous Koopman eigenvalues during the solver iterations for 100 different initial conditions. Since the optimization is always done in discrete time, the errors were also calculated for the discrete eigenvalues.

8.2 Control of a system with multiple equilibria

In this example, we deal with the damped Duffing oscillator with forcing. We will show that we can steer the system into all of its equilibria, including the unstable one, with the KMPC. This maneuver is also possible with other methods for approximating the Koopman predictor, we shall therefore provide a comparison with them, namely EDMD and the Optimal eigenfunction approach from [22].

The continuous dynamics are

$$\begin{aligned} \dot{x}_1 &= x_2, \\ \dot{x}_2 &= -0.5x_2 - x_1(4x_1^2 - 1) + 0.5u, \end{aligned} \tag{87}$$

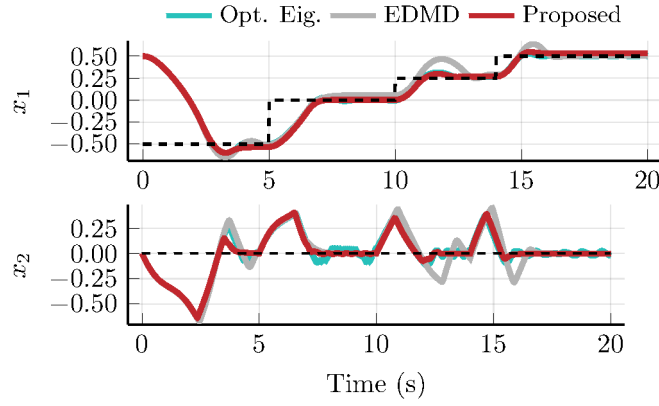
where $x \in [-1, 1]^2$ and $u \in [-1, 1]$. The system has 3 equilibria $x_{e_1} = [-0.5, 0]$, $x_{e_2} = [0, 0]$, and $x_{e_3} = [0.5, 0]$.

For training, we discretize the system (87) using Runge-Kutta 4 with sampling time $T_s = 0.02$ s. We used $N = 100$ trajectories, each containing 1000 samples. The trajectories were split into shorter ones with length $H_T = 20$. The lifted space has size $n_z = 30$ and the input was quantized equidistantly with 11 quantization levels. All of the three methods used the same data, only the Optimal eigenfunctions were learned directly on the long trajectories (since it is beneficial for the method), and the EDMD was learned on pairs of consecutive states. The lifting functions for the EDMD were thin plate splines used in [21]. The dataset had the control-separating properties discussed in 5.1 and proven in the Lemma 2, the EDMD also profited from this as it was able to control the system as well as the other two considered methods.

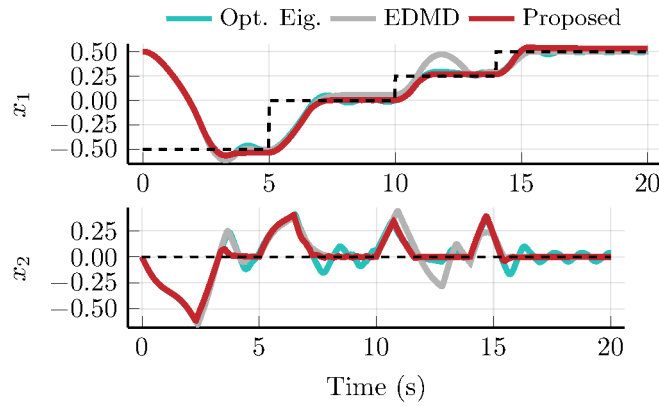
The MPC parameters were $Q = \text{Diag}(15, 0.1)$, $R = 1$, and $H = 60$ (1.2s), $y_{[\text{up}, \text{low}]} = \pm[1, 1]$. The original input bounds were $\Delta u_{[\text{up}, \text{low}]} = \pm 46$ and $u_{[\text{up}, \text{low}]} = \pm 1$. The lifted input bounds were $\Delta v_{[\text{up}, \text{low}]} = \pm 5$ and $v_{[\text{up}, \text{low}]} = [0.108, -0.11]$. Note that the bounds for the lifted inputs depend on the particular initialization of the variables (23). In our case, the function Ψ was *linear* after the optimization (23), approximately $\Psi(u) \doteq 0.1u$.

The Figure 9 shows the three methods on a maneuver which requires to stabilize the system at all three equilibria and the point $[0.25, 0]^T$, which is not an equilibrium. We can see that the EDMD has issues with stabilizing the system at the non-equilibrium point. The Figure 9a shows that the methods are have comparable results apart from the non-equilibrium point.

The Figure 9b shows the same maneuver with a longer prediction horizon which usually leads to better closed-loop performance. We see that the EDMD and optimal eigenfunctions introduce oscillations into the system, making the performance worse, while the proposed method improved its behaviour by smoothening out its overshoots (most visibly around 4s and 11s).



(a) Results for short horizon $H = 20$. All methods are able to control the system, although EDMD has large overshoots and oscillations.



(b) Comparison with longer horizon $H = 60$. Both EDMD and Op. Eig. oscillate around the equilibria.

Figure 9: Comparison of the proposed method, EDMD, and the optimal eigenfunction method. The maneuver visited all three equilibria as well as the state $[0.25, 0]^T$, which is not an equilibrium. The EDMD was the least stable, whereas the optimal eigenfunctions were destabilized only with a large prediction horizon. The proposed method provided the same results for all

8.3 Control with nonlinear input function

In this example, we use the Duffing oscillator with changed control term. The continuous dynamics are

$$\begin{aligned} \dot{x}_1 &= x_2, \\ \dot{x}_2 &= -0.5x_2 - x_1(4x_1^2 - 1) - 0.5u^2, \end{aligned} \tag{88}$$

where the square in the control input is the only change from the previous example. The dataset parameters and the MPC setup are exactly the same as in the previous case. The point of this example is to show that predictors that use the original input u cannot approximate and therefore control certain class of systems, such as (88).

We chose EDMD as a representant of the predictors with original control input and learned it alongside of our method on the system (88). Our method resulted in a predictor with the input lifting function shown in Fig. 10, which is simply a scaled (and shifted) $-0.5u^2$. We attempted to perform a maneuver that would bring the Duffing oscillator from one stable equilibrium to the other, i.e. from $[0.5, 0]^\top$ to $[-0.5, 0]^\top$. The results can be seen in Fig.11. We see that EDMD was not able to leave the equilibrium. The Figure 12 shows the maneuver in a state space plot. We see that our controller exploited the dynamics and did not apply any control when the system was going to the equilibrium on its own (at acceptable rate, we see that the controller sped up the converge near the equilibrium).

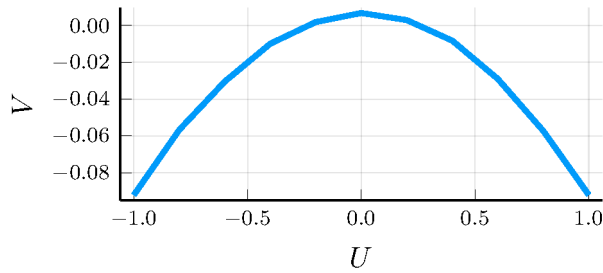


Figure 10: Learned input transformation of a Duffing oscillator with nonlinear control term $-0.5u^2$.

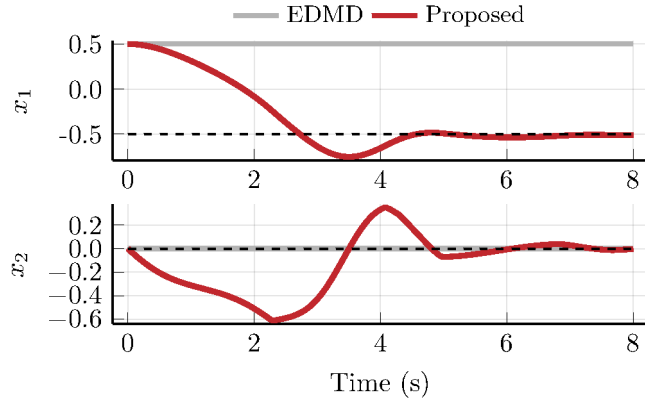


Figure 11: Control of a Duffing oscillator with nonlinear control term. EDMD was not able to leave the equilibrium because the method does not consider nonlinear input transformations.

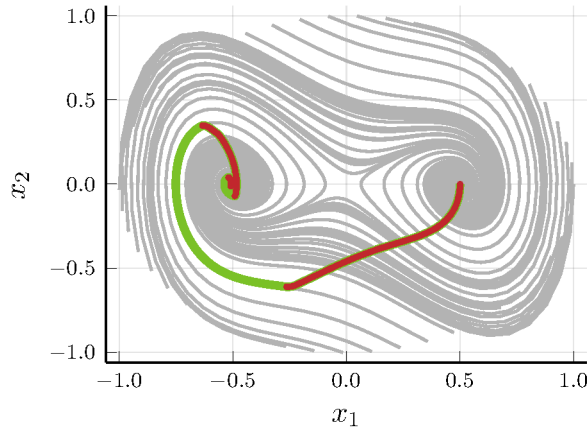


Figure 12: Nonlinear Duffing control trajectory (red/green) plotted over autonomous trajectories (grey) of the system. Control was applied only in the red parts of the trajectory.

8.4 Singletrack vehicle model

This example will show the algorithm on a singletrack vehicle model used in [10]. We shall present open-loop prediction capabilities, show that the lifted variables may have real-world physical meaning, and demonstrate the advantage of using the KMPC over a local-linearization-based MPC (we shall call it Linear MPC from now on).

8.4.1 Model description

Due to the complex nature of the model, we shall present it only as a black-box model and refer the reader to [10, Section 2] for full model derivation. The vehicle is modeled as a planar singletrack

model, also referred to as bicycle model. The main source of nonlinearities are the tires, which are modeled using the high-fidelity "Pacejka tire model (2012)". This tire model contains over a hundred of parameters, which are measured on the physical tire itself. The parameter set used in this work is from the *Automotive Challenge 2018* organized by Rimac Automobili. We refer the reader to [28, Chapter 4] for details on the full tire model.

For our purposes, the vehicle is a nonlinear function

$$\begin{bmatrix} \dot{v}_x \\ \dot{v}_y \\ \dot{r} \end{bmatrix} = f_v \left(\begin{bmatrix} v_x \\ v_y \\ r \end{bmatrix}, \begin{bmatrix} \delta \\ \lambda \end{bmatrix} \right), \quad (89)$$

where the states v_x (m/s), v_y (m/s), and r (rad/s) are the vehicle longitudinal, lateral, and angular velocities in this order. The inputs δ ($^\circ$) and λ (-) are the front steering angle and the rear-tire slip ratio respectively. The bounds on the states and inputs are $v_x \in [0, 30]$ m/s, $v_y \in [-30, 30]$ m/s, $r \in [-15, 15]$ rad/s, $\delta \in [-30, 30]^\circ$, and $\lambda \in [-1, 1]$.

The model was discretized using Runge-Kutta 4 with sample time $T_s = 0.02s$.

8.4.2 Predictor learning

The number of learning trajectories was $N = 8384$ with length $H_T = 10$ (0.2s). A state was considered feasible if its kinetic energy was less than 300kJ, forward velocity v_x was positive, and the front-wheel slip angles were less than 15° . A trajectory was considered feasible if 70% of its states were feasible.

The dimension of the lifted state-space was $n_z = 45$. The vehicle has the following symmetry

$$\begin{bmatrix} \dot{v}_x \\ -\dot{v}_y \\ -\dot{r} \end{bmatrix} = f_v \left(\begin{bmatrix} v_x \\ -v_y \\ -r \end{bmatrix}, \begin{bmatrix} -\delta \\ \lambda \end{bmatrix} \right), \quad (90)$$

which was exploited by the proposed predictor according to the Section 4.

8.4.3 Analysis of the Koopman predictor

Before presenting results of closed-loop control, we would like to show properties of the approximated Koopman operator.

The open-loop predictions remain accurate far longer than the $H_T = 10$ used for learning. The Figures 13 and 14 show trajectories of length $H_{ol} = 100$; the former uses a state from Z_0 as an initial condition, whereas the latter uses a state with non-negligible lifting error. Both examples show good prediction and asymptotic properties, considering the fact that they are 10 times longer than the learning trajectories.

Another notable result are the lifting functions in the Figures 15 and 16: they appear to have a physical meaning. The lifting function of the steering angle (Fig.15) has a shape of a lateral force characteristics under constant acceleration, and the lifting function of the rear slip ratio (Fig.16) has the typical shape of a longitudinal force characteristics. This means that both lifted inputs can be thought of as scaled and shifted forces, which are a major nonlinearity present in the vehicle model.

8.4.4 Control

In this section, we compare the control performance of the proposed KMPC against EDMD, Linear MPC, and Nonlinear MPC. The operating point of the Linear MPC is $x_{op} = [16.7 \ 0 \ 0]^\top$, $u_{op} = [0 \ 0]^\top$ unless said otherwise. The Nonlinear MPC implements the problem (63), with all the bounds and the cost function identical to KMPC, except for the input weight R , as explained below in (91).

The EDMD had the same lifted state space dimension $n_z = 45$ and the lifting was done using thin plate spline radial basis functions [21]. The learning dataset was the same as for the proposed

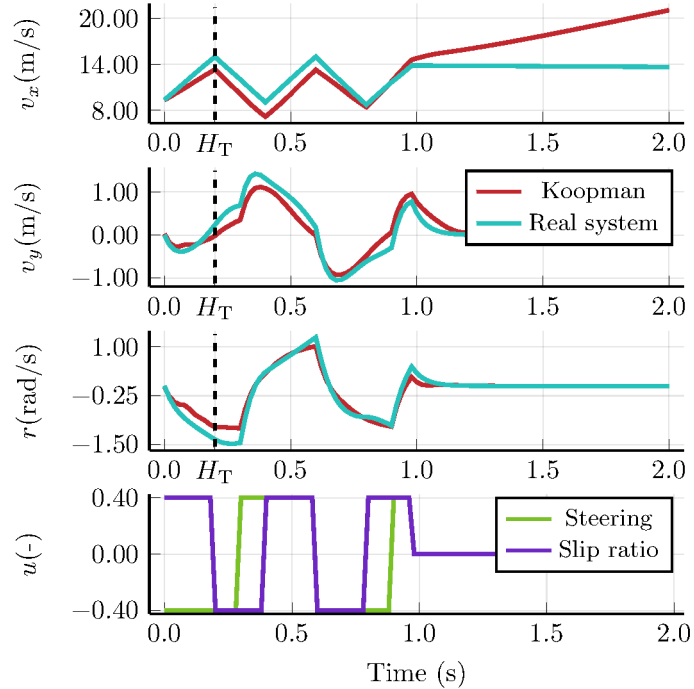


Figure 13: Open-loop prediction with square-wave forcing. The inputs are normalized. The black dashed line shows the learning horizon H_T . The trajectory is 10 times longer than the learning trajectories \mathcal{T}_i . The initial state is taken from the set Z_0 used for learning. The second half of the trajectory shows the asymptotic properties of the predictor; the longitudinal velocity slowly increases, we attribute this to the fact that the predictor is always actuated in the lifted state space (see Fig.16).

method, only scaled to the unit box, as was the case in [21] where the EDMD-based KMPC was first introduced.

In all examples, the MPC parameters were $Q = \text{Diag}(1, 1, 1)$, $R_v = \text{Diag}(300, 30)$, and $H = 30$ (0.6s). The bounds on outputs and inputs were set according to the model description (89).

The input rate constraints were not used in order to make the controllers comparable. All MPCs had the same parametrization, except for the input-weighting matrix R_u , which was calculated by scaling R_v as

$$R_u = R_v \odot s s^\top, \quad (91)$$

where \odot denotes element-wise multiplication and s is a scaling vector, $s_k = (\max(V_k) - \min(V_k))/2$. The scaling was necessary to make the controllers comparable, since the proposed KMPC optimizes the lifted input whereas EDMD, LMPC, and NMPC optimize the original input.

In our previous work [10], we have already presented a Koopman-based MPC for vehicle dynamics but we were not able to outperform the linear controller at all times, only in the highly nonlinear regimes. For this reason, we start with a simple maneuver around an operating point of the Linear MPC, in order to demonstrate that our KMPC is capable of driving the vehicle there.

The first example in Fig. 17 shows a simple maneuver where the car is steered to the left, right, slows down, and finally speeds up. The references are on the yawrate r and velocity v_x . We see

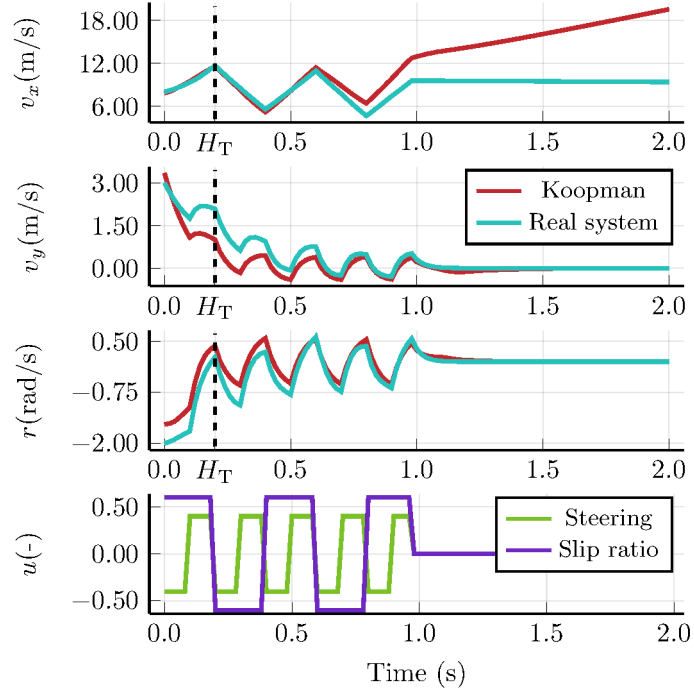


Figure 14: Open-loop prediction with square-wave forcing. The inputs are normalized. The black dashed line shows the learning horizon H_T . The trajectory is 10 times longer than the learning trajectories \mathcal{T}_i . The chosen initial state has noticeable lifting error (the trajectories starts with an offset); in spite of that, the trend of the predicted trajectory is similar to the real one. The asymptotic properties are the same as in Fig.13.

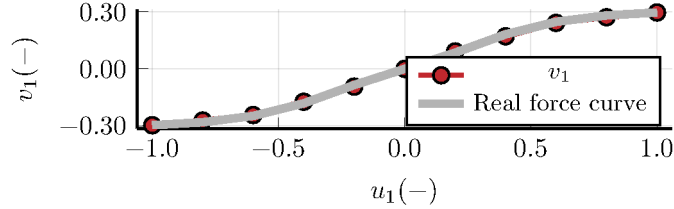


Figure 15: Lifting function of the (normalized) steering angle, compared to scaled lateral force of the front tire at $v_x = 10\text{m/s}$ with slip ratio $\lambda = 0.2$.

that all the controllers track the reference without issues. One can notice the different offsets from the steady-state turns in the beginning of the maneuver. This is likely to be caused by the different weighting of the input mentioned in (91).

The second example in Fig. 18 is stabilization of the vehicle from a sideways skid.

The car starts in sideways skid $x_0 = [0 \quad -15 \quad 0]^\top$ and the goal is to perform a recovery maneuver

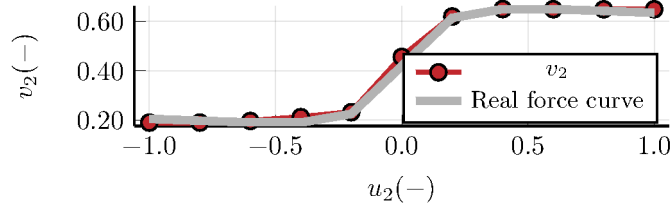


Figure 16: Lifting function of the rear slip ratio compared to a scaled and shifted real force curve of the rear tire for the vehicle driving forward at $v_x = 10\text{m/s}$. Note that the zero of the lifted input is shifted and the lifted input is always positive. We attribute this to the fact that the learning data contained mostly forward-driving states.

and get the vehicle into a forward-driving state $x_{\text{ref}} = [10 \ 0 \ 0]^\top$. The results can be seen in Fig.18. The Nonlinear MPC had the shortest settling time, followed by the proposed method. The linear controller and the EDMD managed to stabilize the system but with much higher cost. Notice also that its yawrate is opposite to that of NMPC, and has much higher peak. Their longitudinal velocities were close to zero until 0.3s mark, which delayed the stabilization.

Figure 19 shows maneuver symmetrical to the one in Fig.18, i.e. the starting state is $x_0 = [0 \ 15 \ 0]^\top$. We see that the EDMD results in a very different trajectory, with v_x very similar to the proposed method and the Nonlinear MPC, although the yawrate still stabilizes late, around the 0.75s mark. All the other controllers resulted in trajectories symmetrical to those in Fig.18.

It is quite surprising and rather undersired that the EDMD performed so differently in two completely symmetrical maneuvers. The proposed method remained consistent in both cases, due to the symmetry exploitation introduced in Section 4.

Timings Table 2 compares the timings of the used controllers. We see that the Koopman, EDMD and the Linear MPCs have comparable computation times. We see that the proposed method seems to have consistent computation time irrespective of the maneuver, unlike the other two linear controllers. Nevertheless, the Linear MPC was the fastest, as expected. The Nonlinear controller is not competitive in terms of timing.

	Proposed	EDMD	Linear	Nonlinear
Fig.19	1.98ms	1.64ms	1.08ms	52.8ms
Fig.18	1.9ms	1.78ms	1.04ms	54.3ms
Fig.17	2.15ms	4.67ms	0.5ms	69.3ms

Table 2: Comparison of average computation times for one MPC iteration. Both Koopman and Linear were solved using OSQP [32] using the dense MPC form found in Appendix A. The Nonlinear MPC used the multiple-shooting formulation [7, 11] designed in CasADi [1] and solved via Ipopt [37]. All simulations were done on Intel Core i7-9750H CPU with $6 \times 2.6\text{GHz}$. The number of cores used by the solvers had negligible effect in all cases.

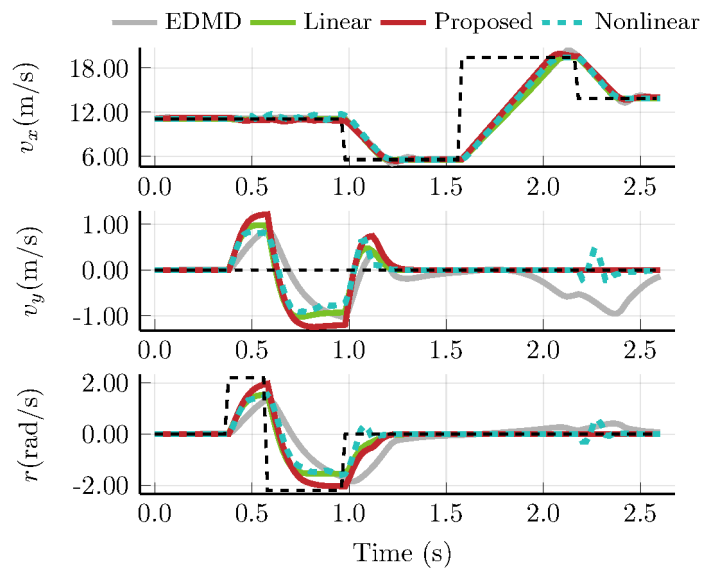


Figure 17: Simple maneuvers around the operating point of the linear controller. The turn radius was 5 meters. Black dotted lines are the references. We see that all controllers performed similarly, although EDMD shows small oscillations by the very end of the maneuver.

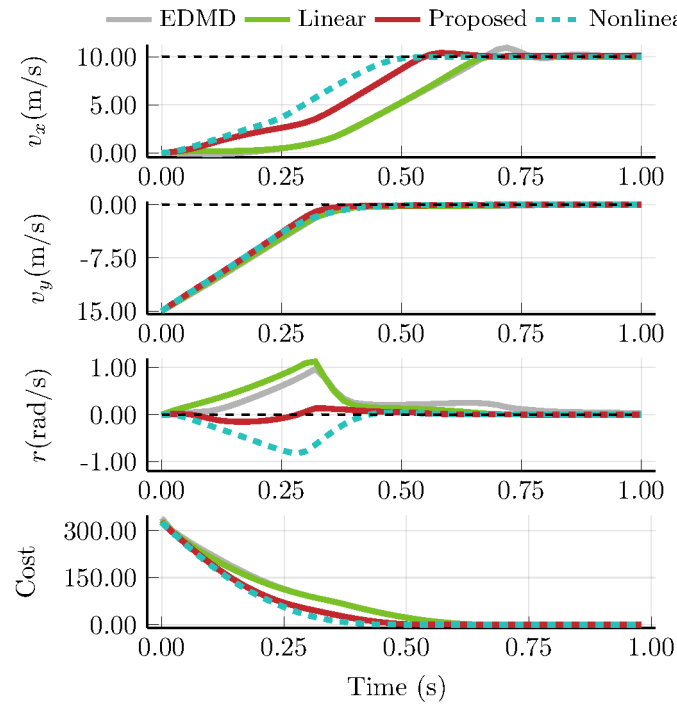


Figure 18: Stabilization of a skidding vehicle. Black dotted line is the reference. Last graph shows the cost function the MPC problem (66). We see that the proposed KMPC and NMPC stabilized the system faster than the other controllers. The Linear MPC performed a maneuver opposite to those of the proposed method and NMPC, had much higher yawrate overshoot, and resulted in significantly higher cost. The EDMD did not manage to stabilize the vehicle in the given time.

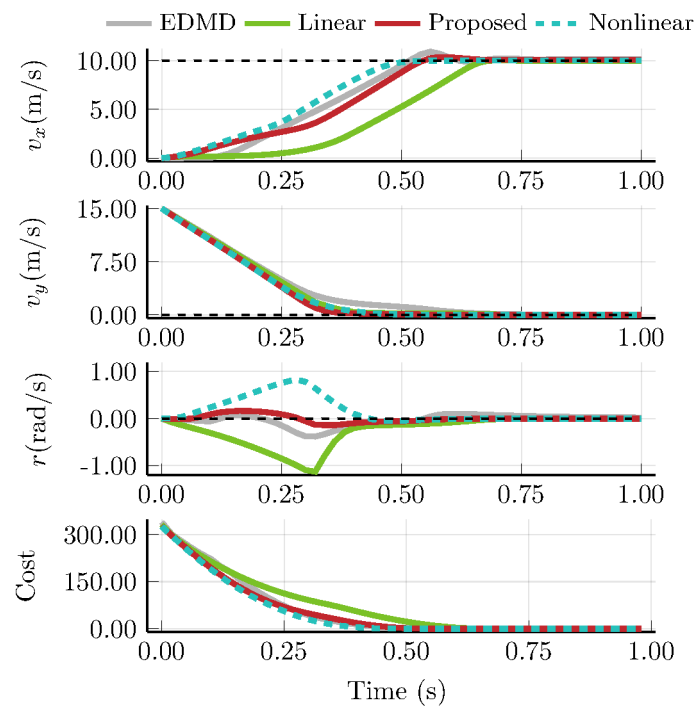


Figure 19: Symetrical maneuver to Fig 18. The EDMD predictor results in a different trajectory than in the previous case from Fig.18, even though the problem setup is symmetrical.

9 Conclusion

We presented a novel method for learning the Koopman predictor of a controlled nonlinear dynamical system. The novelty of this approach consists in searching for both the Koopman predictor and the lifting functions at the same time, as well as in a nonlinear transformation of the control input.

Our examples show that in the classic, autonomous setting, the approach is capable of addressing phenomena such as multiple equilibria and discontinuous lifting functions. We demonstrate that the input transformation allows to control systems which are impossible to control by methods retaining the original input.

In one case, we were able to give physical meaning to the learned input lifting function, without giving any prior information to the optimization routine.

We compared the method to two other Koopman predictors, namely EDMD and Optimal construction of eigenfunctions, to local linearization, and to a nonlinear controller based on CasADi & Ipopt. We show that our method outperforms the aforementioned Koopman approaches, that it can approximate larger class of systems, and that it is competitive to nonlinear control.

Acknowledgments

The authors would like to thank Petar Bevanda for his suggestions regarding the presented examples.

References

- [1] Joel A E Andersson, Joris Gillis, Greg Horn, James B Rawlings, and Moritz Diehl. CasADi – A software framework for nonlinear optimization and optimal control. *Mathematical Programming Computation*, 11(1):1–36, 2019.
- [2] Hassan Arbabi and Igor Mezic. Ergodic theory, dynamic mode decomposition, and computation of spectral properties of the koopman operator. *SIAM Journal on Applied Dynamical Systems*, 16(4):2096–2126, 2017.
- [3] Antonios Armaou and Armin Ataei. Piece-wise constant predictive feedback control of nonlinear systems. *Journal of Process Control*, 24(4):326–335, 2014.
- [4] Craig Bakker, Kathleen E. Nowak, and W. Steven Rosenthal. Learning koopman operators for systems with isolated critical points. In *2019 IEEE 58th Conference on Decision and Control (CDC)*. IEEE, dec 2019.
- [5] Antoine Bambade, Sarah El-Kazdadi, Adrien Taylor, and Justin Carpentier. PROX-QP: Yet another Quadratic Programming Solver for Robotics and beyond. In *RSS 2022 - Robotics: Science and Systems*, New York, United States, June 2022.
- [6] Jeff Bezanson, Alan Edelman, Stefan Karpinski, and Viral B Shah. Julia: A fresh approach to numerical computing. *SIAM review*, 59(1):65–98, 2017.
- [7] H.G. Bock and K.J. Plitt. A Multiple Shooting Algorithm for Direct Solution of Optimal Control Problems. *IFAC Proceedings Volumes*, 17(2):1603–1608, jul 1984.
- [8] Steven L Brunton, Marko Budišić, Eurika Kaiser, and J Nathan Kutz. Modern koopman theory for dynamical systems. *SIAM Review*, 64(2):229–340, 2022.
- [9] Torsten Carleman. Application de la théorie des équations intégrales linéaires aux systèmes d'équations différentielles non linéaires. *Acta Mathematica*, 59:63–87, 1932.

- [10] Vít Cibulka, Milan Korda, Tomáš Haniš, and Martin Hromčík. Model predictive control of a vehicle using koopman operator. March 2021.
- [11] Moritz Diehl. *Real-Time Optimization for Large Scale Nonlinear Processes*. PhD thesis, 2001.
- [12] Michael Garstka, Mark Cannon, and Paul Goulart. COSMO: A conic operator splitting method for convex conic problems. *Journal of Optimization Theory and Applications*, 190(3):779–810, 2021.
- [13] Alfredo Germani, Costanzo Manes, and Pasquale Palumbo. Filtering of differential nonlinear systems via a carleman approximation approach; 44th ieeec conf. on decision and control & european control conference (cdc-ecc 2005). In *Proceedings of the 44th IEEE Conference on Decision and Control*, pages 5917–5922. IEEE, 2005.
- [14] Michael Innes. Don’t unroll adjoint: Differentiating ssa-form programs. *CoRR*, abs/1810.07951, 2018.
- [15] Michael Innes, Elliot Saba, Keno Fischer, Dhairya Gandhi, Marco Concetto Rudilosso, Neethu Mariya Joy, Tejan Karmali, Avik Pal, and Viral Shah. Fashionable modelling with flux. *CoRR*, abs/1811.01457, 2018.
- [16] Mike Innes. Flux: Elegant machine learning with julia. *Journal of Open Source Software*, 2018.
- [17] Diederik P. Kingma and Jimmy Ba. Adam: A method for stochastic optimization. December 2014.
- [18] B. O. Koopman. Hamiltonian Systems and Transformation in Hilbert Space. *Proceedings of the National Academy of Sciences*, 17(5):315–318, may 1931.
- [19] Bernard O Koopman and J v Neumann. Dynamical systems of continuous spectra. *Proceedings of the National Academy of Sciences*, 18(3):255–263, 1932.
- [20] Milan Korda and Igor Mezić. Optimal construction of koopman eigenfunctions for prediction and control. *IEEE Transactions on Automatic Control*, 65(12):5114–5129, 2020.
- [21] Milan Korda and Igor Mezić. Linear predictors for nonlinear dynamical systems: Koopman operator meets model predictive control. *Automatica*, 93:149–160, jul 2018.
- [22] Milan Korda and Igor Mezić. Optimal construction of Koopman eigenfunctions for prediction and control. 2019.
- [23] Qianxiao Li, Felix Dietrich, Erik M Bollt, and Ioannis G Kevrekidis. Extended dynamic mode decomposition with dictionary learning: A data-driven adaptive spectral decomposition of the koopman operator. *Chaos: An Interdisciplinary Journal of Nonlinear Science*, 27(10):103111, 2017.
- [24] D.Q. Mayne, J.B. Rawlings, C.V. Rao, and P.O.M. Scokaert. Constrained model predictive control: Stability and optimality. *Automatica*, 36(6):789–814, jun 2000.
- [25] Igor Mezić. Spectral Properties of Dynamical Systems, Model Reduction and Decompositions. *Nonlinear Dynamics*, 41(1-3):309–325, aug 2005.
- [26] Igor Mezić and Andrzej Banaszuk. Comparison of systems with complex behavior. *Physica D: Nonlinear Phenomena*, 197(1-2):101–133, 2004.
- [27] Samuel E Otto, Sebastian Peitz, and Clarence W Rowley. Learning bilinear models of actuated koopman generators from partially-observed trajectories. *arXiv preprint arXiv:2209.09977*, 2022.

- [28] Hans Pacejka. *Tire and Vehicle Dynamics*. Elsevier LTD, Oxford, 2012.
- [29] Anthony N. Michel Panos J. Antsaklis. *A Linear Systems Primer*. Birkhäuser Boston, 2007.
- [30] Andreas Rauh, Johanna Minisini, and Harald Aschemann. Carleman linearization for control and for state and disturbance estimation of nonlinear dynamical processes. *IFAC Proceedings Volumes*, 42(13):455–460, 2009.
- [31] Anastasiya Salova, Jeffrey Emenheiser, Adam Rupe, James P Crutchfield, and Raissa M D’Souza. Koopman operator and its approximations for systems with symmetries. *Chaos: An Interdisciplinary Journal of Nonlinear Science*, 29(9):093128, 2019.
- [32] B. Stellato, G. Banjac, P. Goulart, A. Bemporad, and S. Boyd. OSQP: an operator splitting solver for quadratic programs. *Mathematical Programming Computation*, 12(4):637–672, 2020.
- [33] Amit Surana. Koopman operator based observer synthesis for control-affine nonlinear systems. In *2016 IEEE 55th Conference on Decision and Control (CDC)*, pages 6492–6499. IEEE, 2016.
- [34] Marko Švec, Šandor Ileš, and Jadranko Matusko. Model predictive control of vehicle dynamics based on the koopman operator with extended dynamic mode decomposition. pages 68–73, 03 2021.
- [35] Marko Švec, Šandor Ileš, and Jadranko Matusko. Predictive approach to torque vectoring based on the koopman operator. In *2021 European Control Conference (ECC)*, pages 1341–1346, 2021.
- [36] Matthew O. Williams, Ioannis G. Kevrekidis, and Clarence W. Rowley. A Data-Driven Approximation of the Koopman Operator: Extending Dynamic Mode Decomposition. *Journal of Nonlinear Science*, 25(6):1307–1346, jun 2015.
- [37] Andreas Wächter and Lorenz T. Biegler. On the implementation of an interior-point filter line-search algorithm for large-scale nonlinear programming. *Mathematical Programming*, 106(1):25–57, apr 2005.

A Condensed MPC formulation

In this section, we show that the problem (66) can be formulated in a way, that makes its size independent of n_z . This is very useful for the Koopman operator, since n_z will be usually large in most applications. We restate the problem (66) for convenience

$$\begin{aligned}
\min_{\Delta v_t, z_t} \quad & \sum_{t=1}^H \|y_{\text{ref}} - y_t\|_Q^2 + \|v_t\|_R^2 + \|\Delta v_t\|_{R_d}^2 \\
\text{s.t.} \quad & z_{t+1} = Az_t + Bv_t \\
& y_t = Cz_t \\
& v_t = \Delta v_t + v_{t-1} \\
& y_{\text{low}} \leq y_t \leq y_{\text{up}} \\
& v_{\text{low}} \leq v_t \leq v_{\text{up}} \\
& \Delta v_{\text{low}} \leq \Delta v_t \leq \Delta v_{\text{up}} \\
& z_0 = \Phi(x_0) \\
& v_0 = \Psi(u_{\text{prev}}),
\end{aligned} \tag{92}$$

where $y_t = \begin{bmatrix} \hat{x}_t \\ \hat{x}_t \end{bmatrix}$, $Q \succcurlyeq 0$, $R \succcurlyeq 0$, and $R_d \succ 0$.

The output trajectory of (92) can be written as

$$\begin{bmatrix} y_1 \\ y_2 \\ \vdots \\ y_H \end{bmatrix} = \begin{bmatrix} CB & & & \\ CAB & CB & & \\ \vdots & & \ddots & \\ CA^{H-1}B & \dots & & CB \end{bmatrix} \begin{bmatrix} v_0 \\ \vdots \\ v_{H-1} \end{bmatrix} + \begin{bmatrix} CA \\ CA^2 \\ \vdots \\ CA^H \end{bmatrix} z_0 \tag{93}$$

or in short as

$$Y = MV + C_z. \tag{94}$$

We see that the size of the matrix M is of size $Hn_y \times Hn_v$ and does not depend on n_z .

The input rates can be obtained as

$$\begin{bmatrix} \Delta v_0 \\ \Delta v_1 \\ \vdots \\ \Delta v_{H-1} \end{bmatrix} = \begin{bmatrix} I & & & \\ -I & I & & \\ & \ddots & \ddots & \\ \dots & 0 & -I & I \end{bmatrix} \begin{bmatrix} v_0 \\ v_1 \\ \vdots \\ v_{H-1} \end{bmatrix} + \begin{bmatrix} -I \\ 0 \\ \vdots \\ 0 \end{bmatrix} v_{\text{prev}} \tag{95}$$

or in short as

$$\Delta V = DV + C_v \tag{96}$$

The first term in the cost function can be rewritten as

$$\begin{aligned}
\sum_{t=1}^H \|y_{\text{ref}} - y_t\|_Q^2 &= (Y - Y_{\text{ref}})^\top Q_H (Y - Y_{\text{ref}}) \\
&= Y^\top Q_H Y - 2Y_{\text{ref}}^\top Q_H Y + Y_{\text{ref}}^\top Q_H Y_{\text{ref}} \\
&= V^\top (M^\top Q_H M) V - 2(C_z - Y_{\text{ref}})^\top Q_H M V + C_0
\end{aligned} \tag{97}$$

where C_0 contains terms that do not depend on V and Y_{ref} is a column vector of y_{ref} repeated H -times. The second term is

$$\begin{aligned} \sum_{t=1}^H \|\Delta v_t\|_{R_d}^2 &= \Delta V^\top R_{d,H} \Delta V \\ &= V^\top (D^\top R_{d,H} D) V + 2C_v^\top R_{d,H} D V + C_1, \end{aligned} \quad (98)$$

where C_1 is a term that does not depend on V .

Finally

$$\sum_{t=1}^H \|v_t\|_R^2 = V^\top R_H V. \quad (99)$$

The total cost can be written as

$$V^\top F V + q^\top V, \quad (100)$$

where

$$F = M^\top Q_H M + D^\top R_{d,H} D + R_{d,H} \quad (101)$$

and

$$q = (-2(C_z - Y_{\text{ref}})^\top Q_H M + 2C_v^\top R_{d,H} D)^\top. \quad (102)$$

The constraints can be written as

$$\begin{bmatrix} M \\ -M \\ I_{H \cdot n_v} \\ -I_{H \cdot n_v} \\ D \\ -D \end{bmatrix} V + \begin{bmatrix} C_z \\ -C_z \\ 0 \\ 0 \\ C_v \\ -C_v \end{bmatrix} \leq \begin{bmatrix} y_{\text{up}} \\ -y_{\text{low}} \\ v_{\text{up}} \\ -v_{\text{low}} \\ \Delta v_{\text{up}} \\ -\Delta v_{\text{low}} \end{bmatrix} \quad (103)$$

or in short as $GV + G_0 \leq h$.

With the formulas (101),(102), and (103) we can write (92) as the following QP

$$\begin{aligned} \min_V \quad & V^\top F V + q^\top V \\ \text{s.t.} \quad & GV + G_0 \leq h. \end{aligned} \quad (104)$$